Feb. 2007
MSc Thesis

ENGINE INSTALLED PERFORMANCE ANALYSIS USING INLET AND EXHAUST DUCT LOSSES GENERATED BY CFD TOOL

CFD 기법에 의해 예측된 흡입구 및 배기구 손실을 고려한
터보 축 엔진의 장착성능에 관한 연구

GRADUATE SCHOOL
CHOSUN UNIVERSITY
Department of Aerospace Engineering

OWINO GEORGE OMOLLO

ENGINE INSTALLED PERFORMANCE ANALYSIS USING INLET AND EXHAUST DUCT LOSSES GENERATED BY CFD TOOL

CFD 기법에 의해 예측된 흡입구 및 배기구 손실을 고려한
터보 축 엔진의 장착성능에 관한 연구

February, 2007

GRADUATE SCHOOL
CHOSUN UNIVERSITY

Department of Aerospace Engineering

OWINO GEORGE OMOLLO

ENGINE INSTALLED PERFORMANCE ANALYSIS USING INLET AND EXHAUST DUCT LOSSES GENERATED BY CFD TOOL

Supervisor Kong Changduk

This thesis is submitted in partial fulfillment of the requirements for the MSc degree in aerospace engineering

November, 2006

GRADUATE SCHOOL
CHOSUN UNIVERSITY

Department of Aerospace Engineering

OWINO GEORGE OMOLLO

GEORGE OMOLLO OWINO

MSc THESIS

Chair	Korea Aerospace Research Institute	Dr. Lee Changho	인
Member	Chosun University	Prof. Kong Changduk	인
Member	Easy Gas Turbine R&D Co., Ltd.	Dr. Ki Jayoung	인

30 November, 2006

GRADUATE SCHOOL

CHOSUN UNIVERSITY

CONTENTS

LIST OF FIGURES

LIST OF TABLES

NOMENCLATURE

CFD	Computational fluid dynamics
D.C	Distortion Co efficient
D.P	Design point
MFP	Mass Flow Parameter
M.N.	Flight Mach Number
MF	Fuel flow
N	Rotational speed
P	Total Pressure
PR	Pressure Ratio
SFC	Specific Fuel Consumption
T	Absolute temperature
t	Centigrade temperature
W	Mass flow, Work
$\dot{m}$	Mass flow
η, h, EFF	Isentropic efficiency
γ	Ratio of specific heats
RPM	Revolutions Per Minute
3-D	Three dimension

Subscripts

a	Air
f	Fuel
c	Corrected
C	Compressor
CC	Combustion Chamber
GG	Gas Generator
g	Combustion gas
m	Mechanical
N	Revolutions Per Minute
O	Oil
PT	Power Turbine
T	Turbine
0	Total
1	Compressor inlet
2	Compressor exit
3	Compressor turbine inlet
4	Power turbine inlet
5	Power turbine exit

ABSTRACT

ENGINE INSTALLED PERFORMANCE ANALYSIS USING INLET AND EXHAUST DUCT LOSSES GENERATED BY CFD TOOL

by OWINO, GEORGE OMOLLO

Advisor : Prof. Kong, Changduk, Ph. D.

Department of Aerospace Engineering,

Graduate School of Chosun University

This paper describes an advanced simulation strategy in which a couple of steady state high-fidelity three dimension analysis of an engine component, the inlet and exhaust duct aimed at developing a reliable smart UAV capable of high speed cruise, takeoff , and all flight modes that applies to a UAV.

Since the object of study involves advance flight dynamics it is essential that the intake and exhaust system including the plenum chamber be designed with maximum accuracy that facilitate good performance characteristics. hence the purpose of this study being the analysis of inlet and exhaust duct losses experienced in the ducts in question. The losses is then used to analyze installed engine loss.

3-D CFD analysis is employed to calculate the pressure loss and show the flow characteristics through the inlet and exhaust system at different flight attitudes. inlet and exhaust boundary conditions used are the same as those

used in the design point performance analysis done at sea level static condition and at cruise altitude of 10000ft.

Design point simulation was performed by a commercial program (GasTurb 9) to calculate design and off design performance of the candidate gas turbine engine.

Simulation methods are not only costly but also time consuming. Superior simulation and analysis method is hence vital and as shown in this research that alternative method can be used to describe the engine performance with specific detail on the performance of the intake and exhaust so that cost-effective and time management simulation is present for future designs.

ACKNOWLEDGEMENT

I would like to extend my sincere thanks to the course members and staffs at Chosun University for their friendship, support and knowledge they have brought me over the years as l pursue my studies.

It is a privilege to have been taught and guided by experts they have made this years invaluable.

I am indebted and grateful to my supervisor, Dr. Professor Changduk Kong for his insight and advice through the course work and on my Thesis.

In addition I am especially thankful to Dr. Jayoung Ki my adviser at the gas turbine engine laboratory in Department of Aerospace Engineering at Chosun University who saw me through my paper work and tirelessly gave me her professional advice.

I would like to thank the staff at KARI (Korea Aerospace Research Institute) Dr Changho Lee for providing the initial cross-sectional co-ordinate of the inlet duct in question.

And lastly my wife Panadda and Son Marvin Omollo for having given me moral support when things got harder my forever love belongs to them.

Dedicated to my family and parent

1. INTRODUCTION

Advances in Aerospace industry have grown and developed significantly over the years. The competition and huge demand for reliable, cost effective, technologically advanced Aircraft and components has placed pressure on the industry to deliver products quickly and efficiently.

Computational simulations are replacing experimental research and consequently development time and cost are decreasing. The primary role of computational simulation in the engine and Airframe design is to minimize time, cost through the use of theoretical analysis. Additional advantages of computational simulations include the possibility to make design trade-offs before component manufacture and offer less risk of malfunctioning components.

In CFD advanced flow visualization is possible one that is not possible during hardware testing. However though CFD is cost effective and time is short to be skillful in its use. It is time consuming and takes vast amounts of computer memory, power. The performance reliability of 3-D simulation is dependent on the effects of the components upstream and downstream at that station.

In this research a fully integrated commercial program GASTURB 9 is used to obtain design point data used for outlet boundary condition and calculation done at ISA standard used for inlet conditions boundary. CFD program is then used for grid generation and perform flow analysis the CFD output results include-pressure, temperature mass flow (calculated) inlet momentum drag at different reference points within the model simulated.

Both free stream flow simulation and vectored simulation say 4° angle of attack was performed at maximum flight altitude and during take-off.

1.1 Aims and Objectives

This paper describes a method in which high-fidelity 3-D analysis of an engine component the intake and exhaust was analyzed for losses that were later used in the analysis of engine installed loss performance.

The research aims to provide the reader and the industry with a detailed explanation on how components loss analysis may be performed using CFD program a method that may be adopted at the industry level to reduce both cost and time required to analyze a given component.

The study analyzes the effect on pressure recovery for both the straight and level flight (Free stream) condition and for the distorted case as in take off flight.

The following parameters were used during the initial CFD analysis altitude (sea level)～10,000 ft (3048m) Mach 0～0.4.

The distortion case include the following flight condition parameter which have been chosen in order to reproduce a typical flight free stream flight Mach 0.4 altitude 3048m 4° angle of attack Mach 0.4 altitude 0.

During the research CFD was used as a means of testing the data and providing the user with visual analysis of the progress made in the loss analysis. It is through CFD analysis that phenomena such as flow separation and distortion can be realized and where necessary corrected.

1.2 Simulation Techniques

The chosen engine design point analysis is performed in order that preliminary boundary conditions are got and used in CFD program. The design point analysis in this study was performed by the use of a commercial program GASTURB 9 however though data from the engine manufacturer may be used if available.

This study hence focuses on the analysis of inlet loss, flow distortion and on the pressure recovery of a UAV (Unmanned Aerial Vehicle) inlet and exhaust ducts developed by Korea Aerospace Research Industry K.A.R.I. together with installed engine loss incurred as a result of using this ducts.

Take off; engine performance data and condition whose parameters are stated and outlined in the previous chapters were used throughout this study.

The engine operating condition, power setting and flight condition are selected and steady state simulation performed using GASTURB 9 to generate an initial set of inlet and outlet boundary condition.

Upon convergence, the data can be used with appropriate functions for more accurate, estimate of the component performance the fully defined characteristics replaces the default data. These boundary conditions define the boundary conditions used in the 3-D model. The input and output parameters can be summarized in steps.

Figure 1 below illustrates the key stages that was used to derive various boundary input condition.

The Figure 2 below shows the schematic arrangement of inlet, engine and exhaust duct assembly used in this research with plenum chamber fitting on the side intake of the engine specified Pratt and Whitney turbo shaft engine PW206C engine.

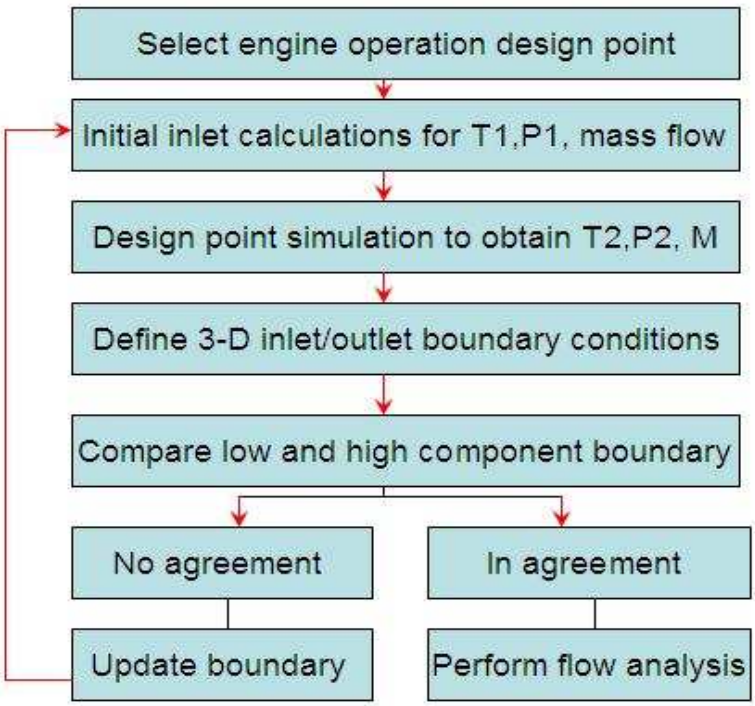

Figure 1. Fully Integrated intake boundary layer deriving technique

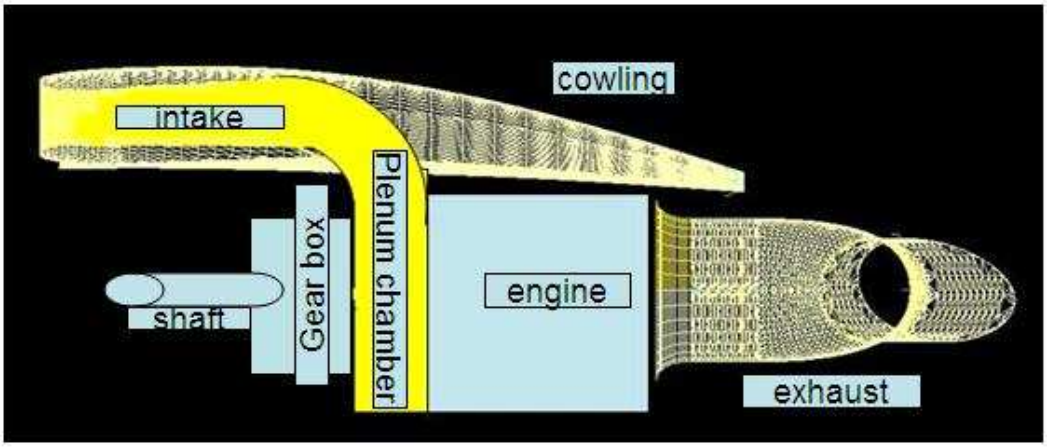

Figure 2. Schematic diagram of inlet, engine and exhaust assembly

2. LITERATURE REVIEW

2.1 Research on Intake and Exhaust Simulation

Although simulation on intake and exhaust has been done for years like the use of Numerical propulsion system simulation (NPSS) developed by NASA, industry, government agencies and universities to create an advanced complete simulation system to perform detailed full engine simulations.

Analysis using CFD method is a relatively new idea that's still under development for use in aeronautical vehicle propulsion system.

John K Lytle discussed a detailed overview of NPSS code in 1999 and stated that extension of the simulation capability from individual engine components to the full system achieves a reduced number of hardware builds and tests during advanced propulsion system development by providing the user with a virtual wind tunnel.

For example, the integration of thermal effects especially heat transfer are important in transient performance simulation. Lytle examined the physical processes within a gas turbine engine and acknowledged that these modeling techniques must include component integration to capture interactions, multidisciplinary coupling to capture the key physical processes, and variable complexity analysis to capture the key physical processes, and variable complexity analysis to minimize the time to solution.

Within the NPSS code objectives, fall several civil aviation requirements. This revitalization includes reduction in aerospace products development time, aircraft accidents rate, travel time noise and emissions ownership cost.

2.2 Aerodynamic Factors

The inlet of and aircraft structure is the most forward part of the nacelle it is through the intake, that the gas turbine is supplied with a high quality flow of air from the atmosphere. The air in the atmosphere at a distance far ahead of the aircraft is from an undisturbed condition, upstream infinity as the aircraft moves towards this air the quantity, the air is divided into two streams.

The first stream, internal flow is that which passes through the intake and is required to reach the engine face with optimum pressure and flow uniformity, thus maximizing performance and stability of engine operation. This flow is characterized by mass flow rate, pressure recovery, distortion, angular flow and stability.

The external flow has a great influence on aircraft aerodynamics and effects must be determined and analyzed during design stages. Internal flow is particularly characterized by mass flow rate, pressure recovery, distortion, flow stability. The intake has additional task of decelerating the flow to a point where optimum performance is realized without formation of shock waves.

The upper cross-section of the intake geometry is depicted on Figure 3 below described as follows:

- Cowl: The exterior curve that covers the inner section of the intake successful design prevents flow separation at low mass flow rate & high angle of attack.
- Crest: The part of the exterior curve also called the lip.
- Throat: The part of the interior curve at which the internal radius is the minimum.
- Diffuser: The interior curve that reaches from the lip to the compressor face. By increasing the area of the intake along the length of the diffuser the flow speed is limited to a value that prevents compressor stall.

- Lip: The part of the interior that reaches from the highlight to the throat it prevents separation inside the intake that can stall the compressor.

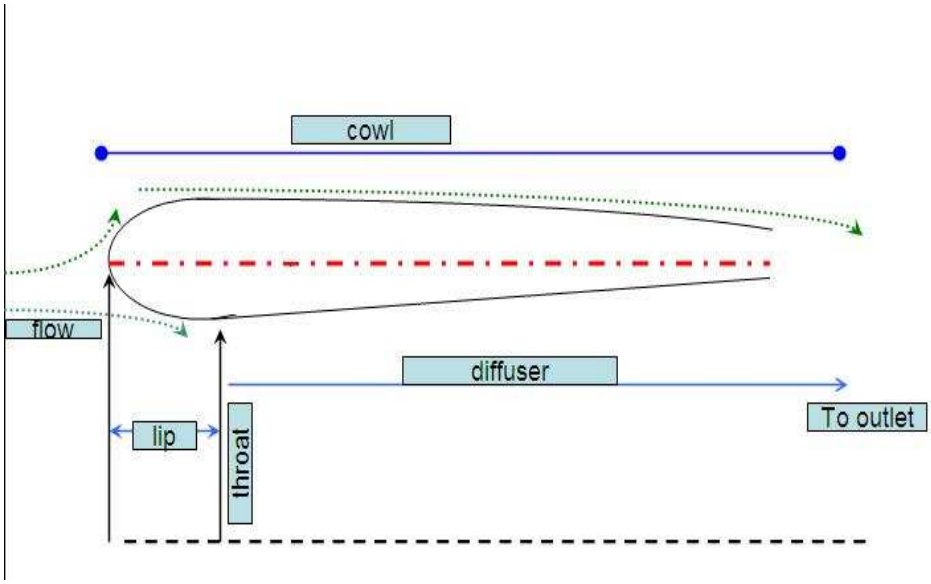

Figure 3. Cross-sectional area of inlet geometry

The above figure shows a standard subsonic cross-section of an intake duct with geometry naming as used in aerospace.

2.3 Diffusers

The purpose of a diffuser is to recover or increase the static pressure. The recovery of pressure realized by a diffuser if predicted by a co-efficient C_p.

$$C_p = \frac{\Delta p}{q_1} \qquad \text{Eqn. 1}$$

q_1 =Inlet dynamic pressure

Δp =Increase in static pressure through diffuser

2.4 Screens

Screens are often used in gas-turbine intake ducting to keep foreign objects out. The pressure loss across a screen placed normal to the flow is given by co-efficient K_s.

$$K_s = \frac{\Delta p}{q} \qquad \text{Eqn. 2}$$

Δp =Pressure loss across screen

q = dynamic pressure based on the average velocity in plane of the screen. This co-efficient is dependent on Reynolds number and screen solidity S

Where

$$s = \frac{blocked\ldots Area}{Total..cross\ sec\ tional..Area} \qquad \text{Eqn. 3}$$

At a given station, mass flow rate

$$m = \rho V A \qquad \text{Eqn. 4}$$

ρ = density

V = velocity

A = cross-sectional Area

As intake ducts are highly dependent on mass flow rate it is vital that during development of duct that the mass flow rate is calculated with the highest accuracy.

It is important that the internal mass flow rate does not reach speeds at which compressor stall occurs the intake hence should act as a compressor to reduce the air relative speed and increase the static pressure.

For example at take off the static pressure at the compressor face (Intake Outlet) drops and the air is accelerated into the intake through suction. Although pressure loss is quantified in terms of total pressure the term pressure recovery is taken as the loss in total pressure between the intake outlet and free stream values. Pressure recovery can be predicted and analyzed. that occurs when pressure across the intake falls due to losses in the flow.

Losses occur in boundary layer regions of flow separation. the pressure recovery of an intake depends on several factors including intake geometry, aircraft speed, engine demands and aircraft maneuvers. It is a measure of efficiency and is valid at all flight speeds.

2.5 Mass Flow Rate Through a Flow Field

The definition of mass flow rate is taken by considering a given area A (Effective Area of Intake) if the area is oriented in the flow field figure 4 below.

The velocity V across the area is taken to be uniform, and the fluid elements with this velocity that pass through area A are considered in time dt after crossing A, the elements have moved a distance Vdt and have swept out the shaded area shown (Figure below).

The volume is equal to the base area A, multiplied by the height of the cylinder $V_n dt$. Where V_n is the component of velocity normal to A.

i.e. $$\text{Volume} = (V_n dt)A \qquad \text{Eqn. 5}$$

The mass inside the shaded area is therefore

$$\text{Mass} = \rho(V_n dt)A \qquad \text{Eqn. 6}$$

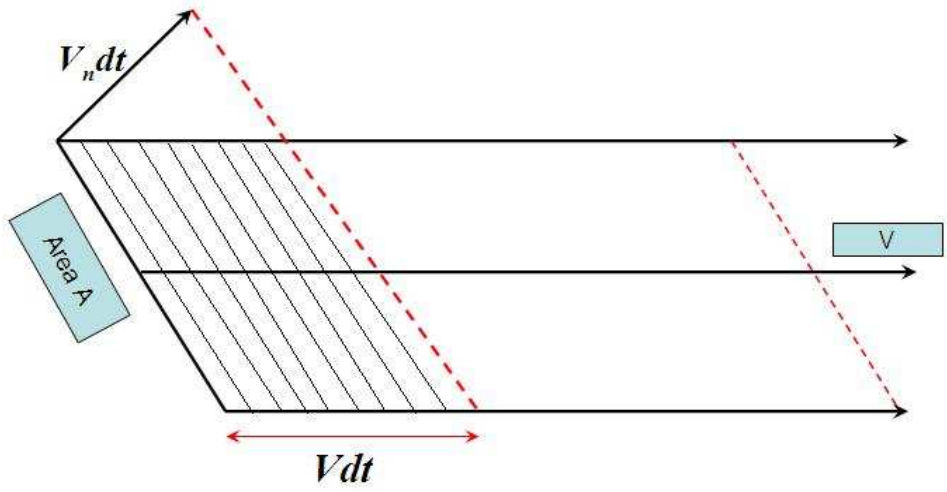

Figure 4. Mass flows through area A in a flow field

This is the mass that has swept past A in time dt. by definition, the mass flow rate through A is the mass crossing area A per second.

Denoting mass flow rate as M

$$M = \frac{\rho (V_n dt) A}{dt} \qquad \text{Eqn. 7}$$

Gives:

$$M = \rho V_n A \qquad \text{Eqn. 8}$$

As the velocity V, across the given area is made up of x, y, and z components of velocity, if the area-plane is rotated, then the actual velocity normal to the area is then the cosine component of that velocity.

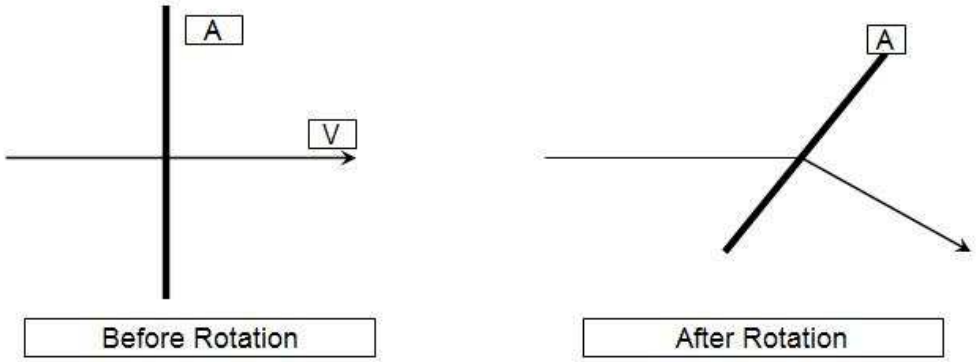

Figure 5. Component of Velocity through A before and After Rotation of θ Degrees

The new velocity through the area is the cosine of original then mass flow rate becomes.

$$m = V \cos\theta . A \qquad \text{Eqn. 9}$$

For example at 4° angle of attack during take-off flights the captured mass flow rate becomes.

$$m = V \cos 4 . A \qquad \text{Eqn. 10}$$

3. INLET PERFORMANCE

3.1 Pressure Recovery

Since pressure recovery is a most important performance parameter in intake aerodynamics, analysis of the loss inside the intake as the airflow enters and reaches the compressor face is of vital importance to tell duct performance.

The total temperature change through the intake of and engine is zero because there is no work done on the internal flow. However the total pressure change varies due to pressure loss between the inlet and outlet of the intake is characterized by pressure recovery $\frac{P_{01}}{P_a}$. Where P is the total pressure and (01) and (a) are the stations numbers respectively. At subsonic flights the losses due to pressure are the only losses and can be related to the two most commonly used ways of expressing intake efficiency are isentropic efficiency, η_i and the ram efficiency η_r (in terms of pressure rise).

For Mach numbers less than 1 the value of recovery is equated to isentropic efficiency η_i defined as the fraction of the inlet dynamic Pressure equated as

$$PRF = \frac{P_{01}}{P_a} = [1 - \eta_i \frac{\gamma - 1}{2} M_a^2]^{\frac{\gamma}{\gamma - 1}} \qquad \text{Eqn.11}$$

Ram efficiency defined as

$$\eta_r = (\frac{p_{01} - p_a}{p_{0a} - p_a})^{\frac{\gamma}{\gamma - 1}} \qquad \text{Eqn.12}$$

In terms of total pressure

$$\frac{\Delta P_a}{P_{0a}} = \frac{P_{0a} - P_{01}}{P_{0a}} \qquad \text{Eqn. 13}$$

and

$$P_{0a} = P_a\left(1 + \frac{\gamma - 1}{2} M_a^2\right) \qquad \text{Eqn. 14}$$

Inlet total % pressure loss

$$\frac{\Delta P_0}{P_{0a}} = 100 * (1 - \eta_r) * \frac{P_{0a} - P_a}{P_{0a}} \qquad \text{Eqn. 15}$$

Equation 12 below describes the mass flow ratio in terms of cross sectional area ratio when this ratio is small there is risk of spillage drag.

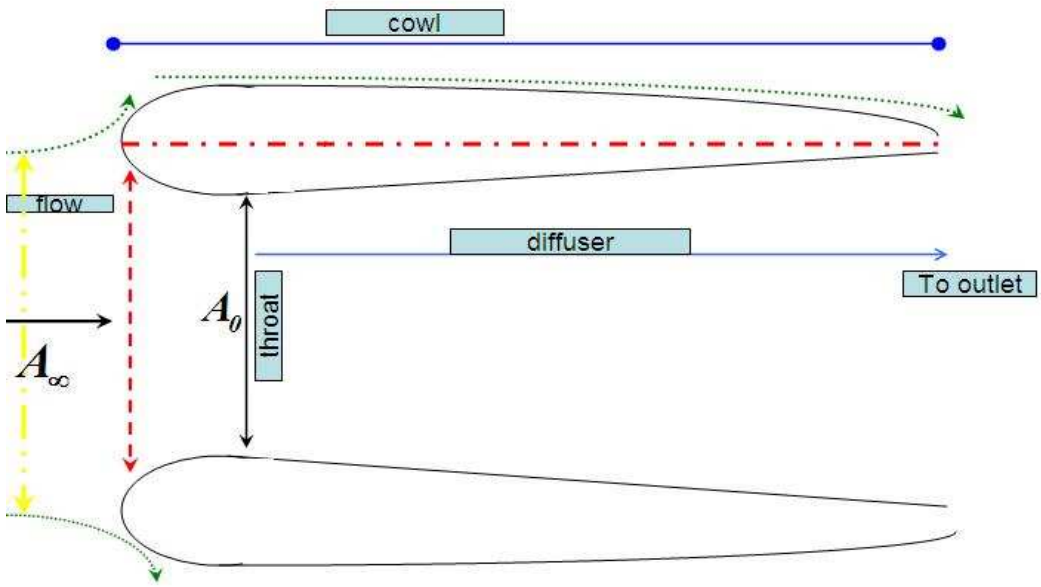

Figure 6. Intake geometry definition

3.2 Mass Flow Ratio

The mass flow ratio describes the behavior of an intake for a given off-design condition. It affects is affected by power setting and Aircraft speed. Thus decreases as power setting or Aircraft speed decrease. The mass flow ratio is determined as:

$$m = \frac{A_\infty}{A_0} \qquad \text{Eqn. 16}$$

Where A_∞ = Cross-sectional area at an infinite distance from the intake.

A_0 = Cross-sectional area of intake duct.

3.3 Sources of Distortion and Turbulence

Distortion is determined at the compressor face. It is a measure of the non-uniformity of the Airflow as it reaches the compressor entry part of the engine.

The sources of inlet flow distortion include flow separation, ingestion of Aircraft vortices (cross winds stall and maneuvers as side slip) lip flow separation due to high angle of attack.

In separated flow conditions intake distortion can be highly turbulent and have eddy sieges large enough to contribute to uneven distribution of total pressure at the engine face that may lead to compressor surge and performance loss.

One portion of the flow may have a higher velocity or higher pressure than the other causing swirling flow or some section of the boundary layer may be thicker because of the intake shape.

This changing flow can cause flow separation in the compressor cause structural damage of blades. A good intake design will smooth out flow have high pressure recovery, low spillage drag and low distortion. Local velocity variations

may be interpreted as local variations in angle of attack of the compressor face flow.

An often used measure of flow quality or flow distortion is given by distortion parameter.

$$DC_{\theta} = \frac{P_f - P_{\theta sector}}{q_f} \qquad \text{Eqn. 17}$$

P_f =overall mean total pressure

P_{θ} =mean total pressure in sector

q_f =engine inlet isentropic pressure

4. COMPUTATIONAL MODELLING

4.1 Engine selection

The engine of choice in this study is the PW206C turbo shaft engine from Pratt and Whitney Canada its use in the development of unmanned Ariel vehicle (UAV) by K.A.R.I has led to this research and analysis to ensure successful use in a UAV system.

4.2 Engine description

It is a free-turbine turbo shaft engine that comprises a single stage centrifugal compressor driven by a single-stage turbine and a single free turbine driving the output shaft through a front-mounted reduction gear box with aluminum inlet and gearbox casing.

This engine is forward facing with side intake that requires the use of a plenum chamber to deliver air onto the compressor face.

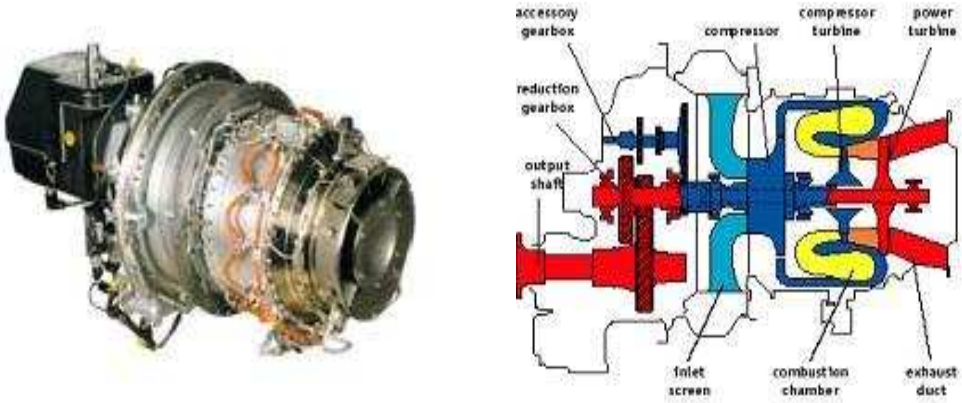

Figure 7. PW206C engine

Table 1. Operating range for propulsion system

Gas generator RPM	65% ~ 100%
Altitude (ft)	0 ~ 15000
Flight Mach No	0 ~ 0.4

Table 2 shows the performance characteristics (default data) with no intake or exhaust pressure loss.

Table 2. Design Performance Data Provided by Engine Manufacturer

Atmospheric condition	Sea Level Static Standard	Alt. = 10000ft, Static Standard
Mass flow rate lbm/s	4.418	3.307
Fuel flow rate lbm/	0.087	0.0724
Compressor pressure ratio	7.912	9.82
Turbine inlet temp	2258	2388
SFC (lbm/hp hr)	0.556	0.5260
Shaft horse power	560.8	496.0

This table 2 represents estimated performance data as give by the manufacturer.

4.3 Design Point Simulation Input Data

A commercial design and off design point simulation program GASTURB 9 was used to perform preliminary design point simulation. Input data includes both the default, design point data that are optional, off-design flight condition data for example varying altitude or Mach number.

For purposes of this research, the design point data includes default values for

the individual component performance characteristics inside the engine and based on engine data available to the public domain Table 2.

The design point data is matched with the take-off data using GASTURB 9 in order to get the output data to obtain correct take-off net thrust and TET.

4.4 GASTURB 9

The software is the executable file form of an interactive FORTRAN program for the design and analysis of gas turbine engine and propulsion system it is a PC/DOS program that analyze the operation of a user specified system having several input parameters value, efficiencies, low and high, limiters of the following:

- Compressor
- Turbine
- Diffuser
- Nozzle
- Mach number
- Ambient conditions

Having these inputs the program calculates both the design and off design points of the engine using scaled components maps factor of known engines however specific maps may also be used if inputted in the appropriate format.

4.5 EEPP (Estimated Engine Performance Program)

This is a program supplied by the engine manufacturer that gives the engine operating point parameters at different flight and altitude conditions.

It works by giving command of the input file data name and a corresponding out put data file is developed by the program showing manufacturers specified value of the engine state at different operating conditions.

4.6 3-D Grid Generation

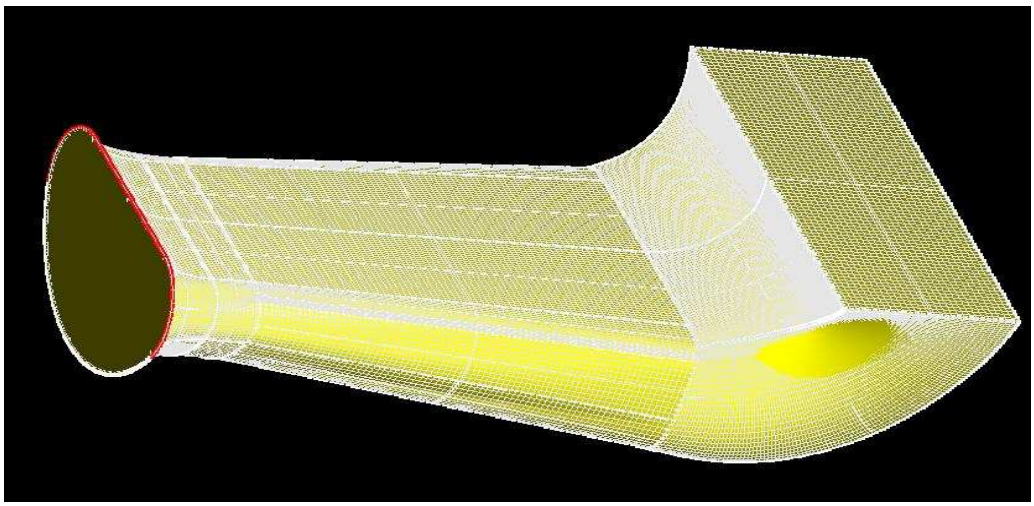

Figure 8. Structured surface grid of the inlet duct

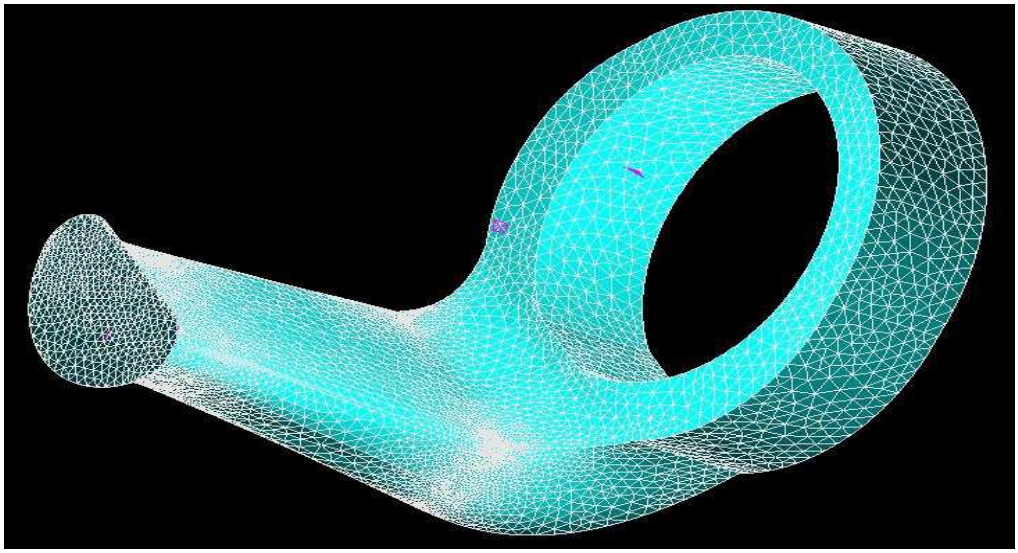

Figure 9. 3-D tetrahedral volume grids

CFD tool GEOM was used to model the duct and to generate both surface and volume grid. The initial geometry data was kindly offered by KARI where the coordinates points received was mapped into the x, y and z axes to form a 3 dimensional continuous edge.

Once the intake geometry is modeled the process of grid generation starts.

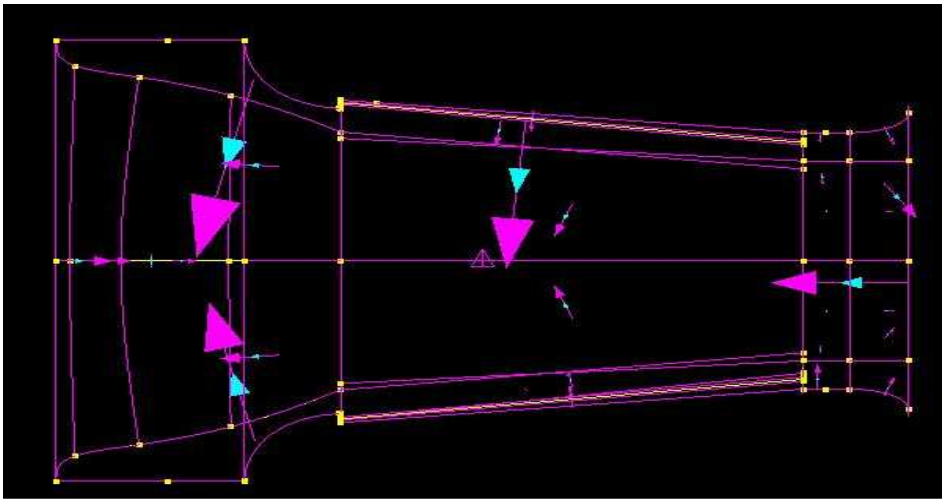

Figure 10. Loop and trim generation

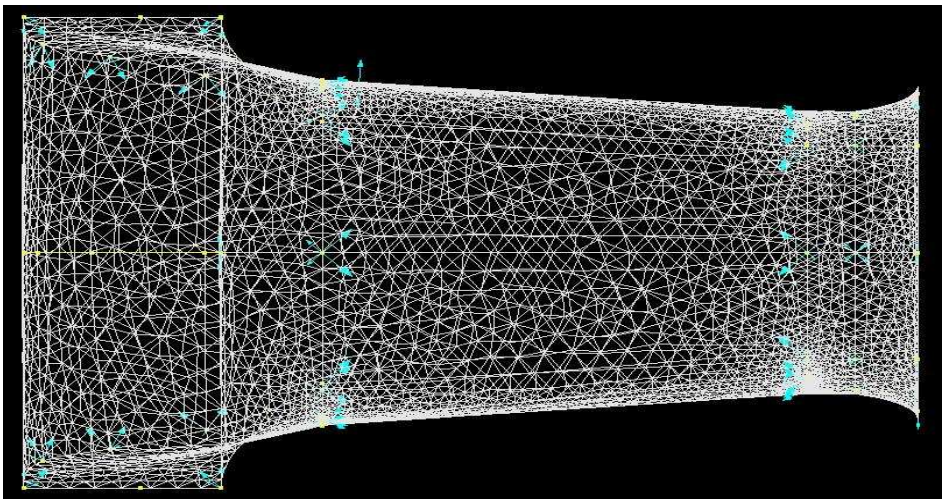

Figure 11. Surface mesh generation

Grid generation starts which involves formation of grid node points, surfaces, loops and trims domain for volume mesh as seen on figure 10 and 11 above. Structured grid was chosen for this research as it has the highest degree of accuracy although takes more simulation time. CFD simulation is strongly linked to the quality of the mesh within the grid.

A more refined Mesh is able to reduce losses whereas a coarse due to high friction loss co-efficient. Tetrahedral volume mesh was used that produced 61034 elements.

As aircraft internal intake surface require a refined and smooth surface Reynolds Navier-strokes(RANS) together with wall functions standard $k-\epsilon$ model and Kato launder $k-\epsilon$ model were used as a way of trying to reduce friction coefficient.

The complete meshed model is the imported into CFD solver (ace) and the final stage in the meshing process include the addition of boundary layers along the surface of the geometry to create inlets and outlets these boundary conditions are illustrated below on Table 3 and include pressure inlet and outlets.

5. PROCEDURE TO DERIVE INTAKE BOUNDARY PARAMETERS

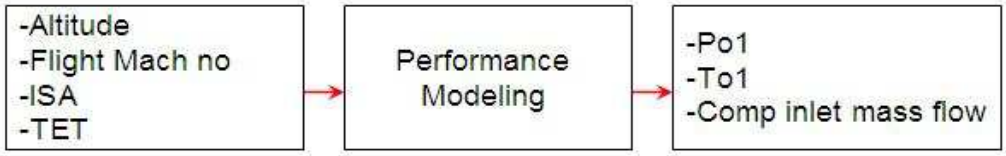

Figure 12. Procedure to derive inlet boundary conditions

Flight altitude, flight Mach number are given on Table 1 above TET obtained from design point simulation and ISA conditions are calculated.

Table 3. Duct boundary conditions parameters same as those used at design point simulation at operating altitude of 10000ft at Mach 0.4

Far-field	Ambient Static Pressure	Pressure	Density
Inlet	Static Pressure	Mass flow rate	Temperature
Outlet Nozzle	Total Pressure	Static Pressure	Temperature

For altitudes below 11000ft then

$$T_{ISA,amb} = 288.15\,K - 6.5 * \frac{alt}{1000\,m} \qquad \text{Eqn. 18}$$

Ambient pressure at this altitude is found by

$$p_{amb} = 101.325\,kPa * (1 - \frac{0.0225577 * alt}{1000\,m})^{5.25588} \qquad \text{Eqn. 19}$$

The velocity of sound depends on static temperature and gas

$$V_{sonic} = \sqrt{\frac{c_p}{c_p - R} * R * T_{amb}} \qquad \text{Eqn. 20}$$

The flight velocity and total temperature

$$V_0 = M_0 * V_{sonic} \qquad \text{Eqn. 21}$$

Is calculated from the total enthalpy

$$H_0 = h(T_{amb}) + \frac{V_0^2}{2} \qquad \text{Eqn. 22}$$

From ambient pressure we can obtain the value of inlet pressure as

$$P_0 = P_{amb} * e^{\psi(T_0) - \psi(T_{amb})} \qquad \text{Eqn. 23}$$

Table 4. Far-field ambient boundary conditions at 10000ft

Altitude (ft)	Temperature (K)	Pressure (Pa)	Density (Kg/m^3)	Sonic Vel. (m/s)	Viscosity (m^2/s)
10000	268.67	70121	0.909	328.58	1.86*10^-5

This represents the environmental condition at an altitude of 10000 based on international standard atmosphere(ISA) calculation.

5.1 CFD Background

Computational fluid dynamics is a numerical tool for simulating the complicated fluid flow, heat transfer and chemical reactions.

This tool has been gaining popularity in recent years due to a number of factors. Dramatic increase in computer power available now in homestead due to low prices. Each new generation of computer hardware continue to have more speed and more memory at low cost.

The improvements in the physics and sub models that are available to user it is possible to model compressible and incompressible, viscous and non-viscous, laminar and turbulent, high and low pressure, reacting and non-reacting, multiphase and other types of flow.

CFD modeling can be used to dramatically reduce the cycle times for developing new products by rapid simulation and a wide range of configurations which would be both time-consuming and expensive to make a prototype. CFD modeling can also be used to scale-up laboratory or field results from one specific application to another type of application.

6. CONSERVATION PRINCIPLES IN FLUID DYNAMICS

The equations that govern fluid flow are based on three conservation laws:

- Mass which is expressed through a continuity equation
- Momentum, which is expressed through a form of Newton's second law
- Energy which is expressed through the first law of thermodynamics

The fundamental equations, need to be combined with other equations that establish relationship between various fluid properties in order to close the system of equations.

CFD solver, GEOM Solver ,Conservation equations for Mass and Momentum for all flows in the case of flow involving heat transfer of compressibility an additional equation for energy is solved then depending on the flows, more equations can be solved.

6.1 Conservation of Mass

The equation for conservation of mass or continuity equation, can be written as

$$\frac{\partial \rho}{\partial} + \frac{\partial}{\partial x_i}(\rho u_i) = S_m \qquad \text{Eqn. 24}$$

Where ρ =density and U_i =velocity in x direction.

This is the general form of continuity equation and is valid for incompressible flow as well as compressible flows.

The source S_m is the mass added to the continuous phase from the dispersed second phase (e.g. due to vaporization of liquid droplets) or any user-defined sources.

6.2 Conservation of Momentum

Newton's second law states that the rate of change of momentum of a fluid particle corresponds to the sum of the forces on the particles.

Two types of forcers on fluid particles are distinguished. The surface forces pressure forces and viscous forces.

The body forces gravity force Coriolis forces and electromagnetic force.

A normal stress is noted by ρ and the viscous stresses are noted by τ body forces are included by using a source term S_{mi} of i-momentum per volume per unit of time.

In Cartesian co-ordinates, the momentum equation can be written as

$$\rho \frac{Du}{Dt} = \frac{\partial(-p+\tau_{xx})}{\partial x} + \frac{\partial \tau_{yx}}{\partial y} + \frac{\partial \tau_{zx}}{\partial z} + S_{mx} \qquad \text{Eqn.25}$$

$$\rho \frac{Dv}{Dt} = \frac{\partial \tau_{xy}}{\partial x} + \frac{\partial(-p+\tau_{yy})}{\partial y} + \frac{\partial \tau_{zy}}{\partial y} + \frac{\partial \tau_{zx}}{\partial z} + S_{my} \qquad \text{Eqn.26}$$

$$\rho \frac{Dw}{Dt} = \frac{\partial \tau_{xz}}{\partial x} + \frac{\partial \tau_{yz}}{\partial y} + \frac{\partial(-p+\tau_{zz})}{\partial z} + S_{mz} \qquad \text{Eqn.27}$$

Where ρ =density u=velocity, p =normal stress, T =viscous stress and S_m =source mass

6.3 Conservation of Energy

Compressible flows or incompressible flows where heat transfer occurs require the use of an energy equation.

The basis of it comes from the first law of thermodynamics. where In Cartesian co-ordinates the energy equation can be written as

$$\frac{\partial T}{\partial t}+u\frac{\partial T}{\partial x}+v\frac{\partial T}{\partial y}=\frac{k}{\rho C_p}\{\frac{\partial^2 T}{\partial x^2}+\frac{\partial^2 T}{\partial y^2}\}-\frac{\mu}{\rho C_p}[2(\frac{\partial u}{\partial x})^2+2(\frac{\partial v}{\partial y})^2+(\frac{\partial u}{\partial y}+\frac{\partial v}{\partial x})] \quad \text{Eqn. 28}$$

Where T=temperature, k=thermal conducting, C_p =specific heat capacity at constant pressure, ρ =density u=velocity and v=velocity

7. INLET DUCT AREA

Table 5. Inlet duct area

Inlet throat area m^2	0.027
Exit area m^2	0.148

Consider a cruise speed of mach 0.4 (131m/s) at an altitude of 10000ft then from Table 5 above.

The throat velocity is 141m/s and exit 26.39m/s refer to simulation results Table 8 below.

$$\dot{m} = \rho U A$$

(throat) = 3.555 Lb/s

(exit) = 3.555 Lb/s

8. CONVERGENCE

8.1 Iterative Steps to Convergence

New Design point simulation converges with the EEPP data at 10000ft Mach 0 off design simulation is done to get TET as 1549.99R Figure 13 however off design performance done at 10000ft at Mach number 0.4 maximum continuous state with TET=1538.11R is used Figure 14.

```
Station   W         T         P        WRstd      PWSD      =     496.0
 amb              483.01    10.106               PSFC      =   0.52601
  2      3.307    483.01    10.106     4.640     V0        =      0.00
  3      3.307   1030.11    99.246     0.690     FN res    =     33.96
 31      3.307   1030.11    99.246
  4      3.379   2388.00    96.268     1.107     WF        =   0.07247
 41      3.379   2388.00    96.268     1.107     s NOx     =   0.16953
 43      3.379   1930.40    31.648               Therm Eff=    0.26307
 44      3.379   1930.40    31.648               P45/P44   =   1.00000
 45      3.379   1930.40    31.648     3.027     ZWBld     =   0.00000
 49      3.379   1549.99    10.308
  5      3.379   1549.99    10.308     8.328     Incidence=    0.00000
  6      3.379   1549.99    10.308
  8      3.379   1549.99    10.308     8.328     P8/Pamb   =   1.01990
P2/P1 = 1.0000                                   A8        =      85.1
Efficiencies:   isentr  polytr    RNI    P/P     TRQ [%]   =     100.0
 Compressor     0.8000  0.8516  0.775  9.820    eta t-s   =   0.80773
 Burner         0.9700                 0.970    Loading %=    100.00
 HP Turbine     0.8300  0.8102  0.511  3.042    WHDBld/W2=    0.00000
 LP Turbine     0.8200  0.7982  0.239  3.070    WHcl/W2   =   0.00000
 HP Spool mech  0.9800  Nominal Spd    56221    WLcl/W2   =   0.00000
 PT Spool mech  0.9740  Nominal Spd       61    WBld/W2   =   0.00000

  Fuel            FHV     humidity   war2
Generic        18400.0       0.0    0.0000

Composed Values:
   1:  PWSD    =   495.971497
   2:  SFC     =     0.526009
   3:  WF      =     0.072468
   4:  A8      =    85.085106
   5:  W3Rstd  =     0.690035
```

Summary | Stations

Figure 13. Design point convergence at 10000ft Mach number 0.0 ISA

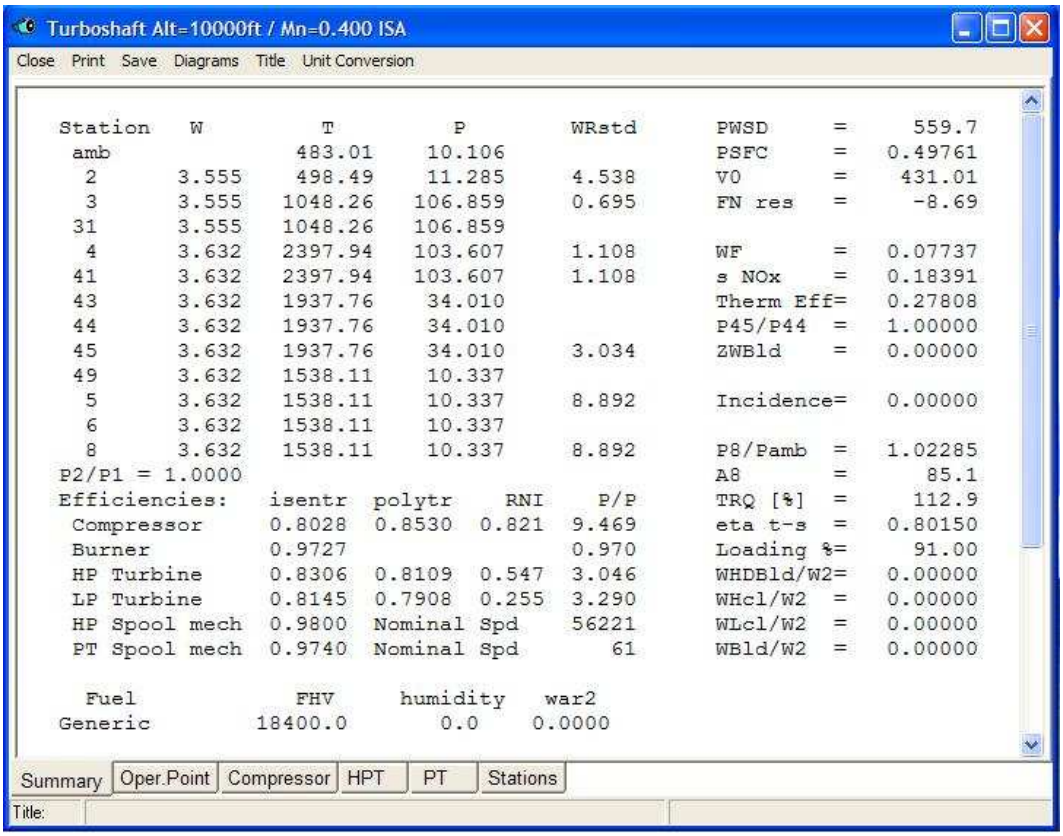

Turboshaft Alt=10000ft / Mn=0.400 ISA

Close Print Save Diagrams Title Unit Conversion

Station	W	T	P	WRstd			
amb		483.01	10.106		PWSD	=	559.7
2	3.555	498.49	11.285	4.538	PSFC	=	0.49761
3	3.555	1048.26	106.859	0.695	V0	=	431.01
31	3.555	1048.26	106.859		FN res	=	-8.69
4	3.632	2397.94	103.607	1.108	WF	=	0.07737
41	3.632	2397.94	103.607	1.108	s NOx	=	0.18391
43	3.632	1937.76	34.010		Therm Eff	=	0.27808
44	3.632	1937.76	34.010		P45/P44	=	1.00000
45	3.632	1937.76	34.010	3.034	ZWBld	=	0.00000
49	3.632	1538.11	10.337				
5	3.632	1538.11	10.337	8.892	Incidence	=	0.00000
6	3.632	1538.11	10.337				
8	3.632	1538.11	10.337	8.892	P8/Pamb	=	1.02285
P2/P1 = 1.0000					A8	=	85.1
Efficiencies:		isentr	polytr	RNI	P/P	TRQ [%]	=	112.9
Compressor		0.8028	0.8530	0.821	9.469	eta t-s	=	0.80150
Burner		0.9727			0.970	Loading %=	91.00
HP Turbine		0.8306	0.8109	0.547	3.046	WHDBld/W2	=	0.00000
LP Turbine		0.8145	0.7908	0.255	3.290	WHcl/W2	=	0.00000
HP Spool mech		0.9800	Nominal Spd		56221	WLcl/W2	=	0.00000
PT Spool mech		0.9740	Nominal Spd		61	WBld/W2	=	0.00000

Fuel	FHV	humidity	war2
Generic	18400.0	0.0	0.0000

Summary | Oper.Point | Compressor | HPT | PT | Stations

Title:

Figure 14. Off-design point maximum continuous 10000ft Mach no 0.4

Table 6. Design point data (EEPP)

Atmospheric condition	Sea Level Static, STD	Altitude=10000ft Static, STD	Altitude=10000ft Mach 0.4, STD
Mass flow rate (lbm/s)	4.418	3.307	3.555
Fuel flow rate (lbm/s)	0.087	0.0724	0.07737
Compressor pressure ratio	7.912	9.82	9.469
Turbine inlet temperature	2258	2388	2397.94
SFC (lbm/hp hr)	0.5560	0.5260	0.4976
Shaft horse power	560.8	496.0	559.7

Table 7. Input boundary conditions based on steady state and off design simulation

Parameter	Station (1)	Station(2)	Ambient conditions
Pressure (psia0	10.106	10.337	10.170
Mass flow rate (lb/s)	3.555	3.555	-
Density (kg/m^3)	0.909	0.909	0.909
Temperature (R)	483.01	1538.11	483.66

Steady state GASTURB 9 simulation provides the outputs as seen on iteration one P_1, T_1 and P_2 are entered as boundary conditions into the 3-D CFD model where(1) and (2) indicate the station number Table 7 Table 6 represents EEPP design point.

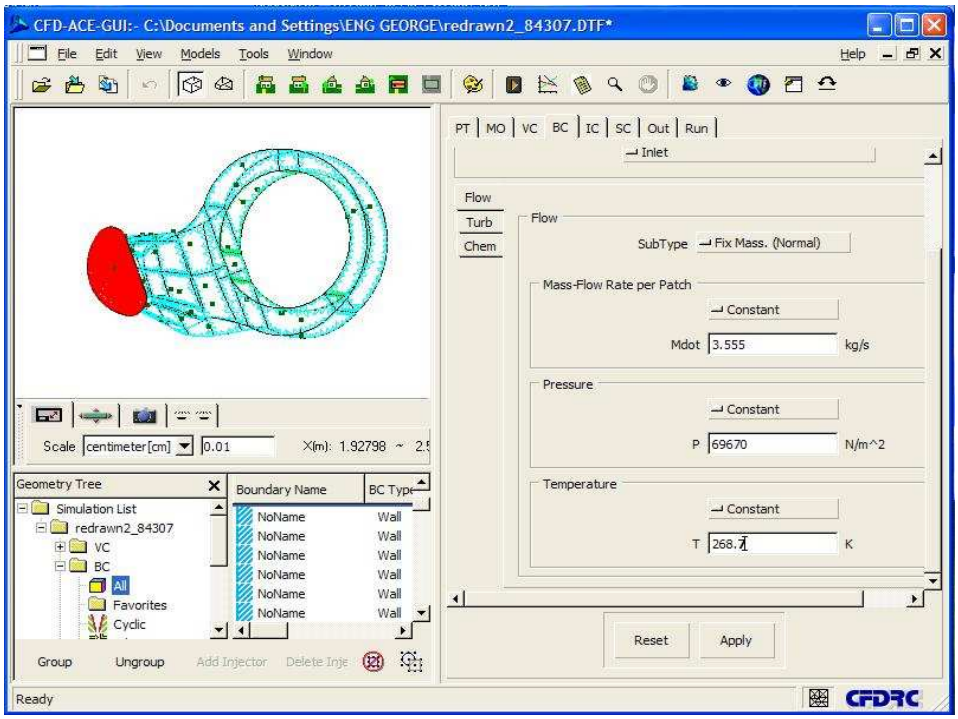

Figure. 15 Far field pressure inlet condition set-up parameter

The figure above shows the CFD ace tool with the inlet face defined. The three boundary conditions for each simulation are set as follows the following example above shows the set-up done at cruise condition of Mach 0.4 at altitude 10000ft.

Far field pressure inlet-P, initial pressure P_1, and total temperature T_1, mass flow rate per patch was set as constant.

$$\dot{m}_{inlet} = \dot{m}_{engine} = \dot{m}_{exhaust} \qquad \text{Eqn. 29}$$

This is in accordance to conservation of mass Eqn 24 above far field outlet consists of pressure P_2, total temperature T_2.

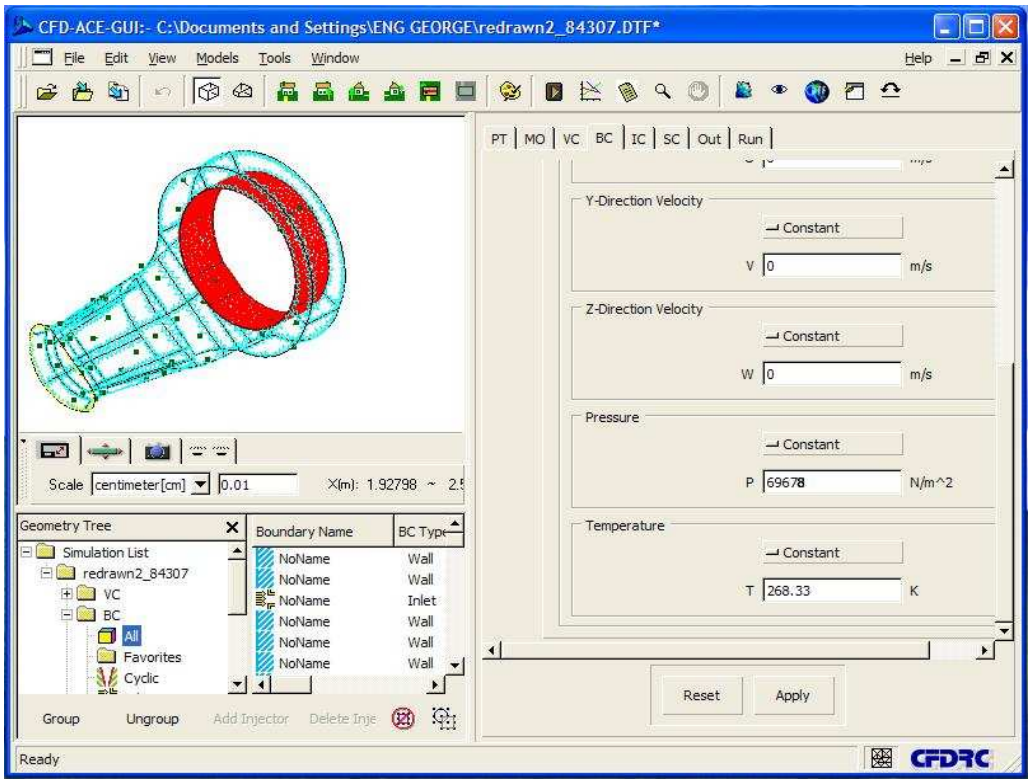

Figure 16. Intake pressure outlet condition set up parameters

Simulation is run and iterations is carefully observed for pressure, velocity and other variable behavior within the ducts .As we can see below Figure 17. There is a slight decrease in pressure and other variable between iteration 0~800.this is an expected trend as the duct being investigated consists of a diffuser section.

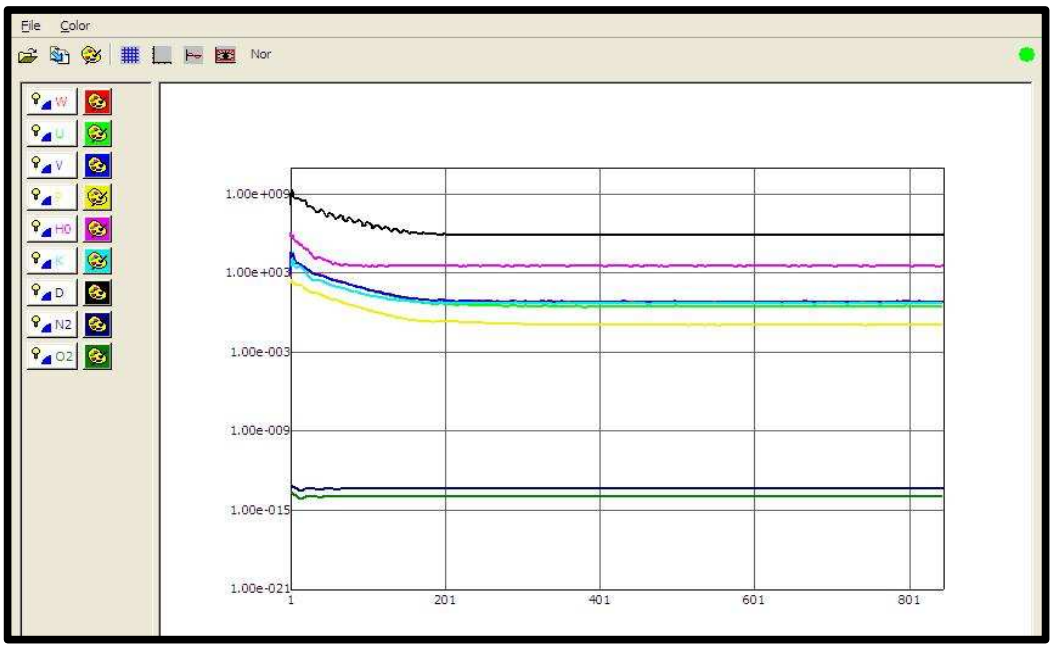

Figure 17. Iteration output

Once simulation is finished data extraction begins using CFD view tool where respective values of pressure, temperature, Mach number can be seen for the selected station.

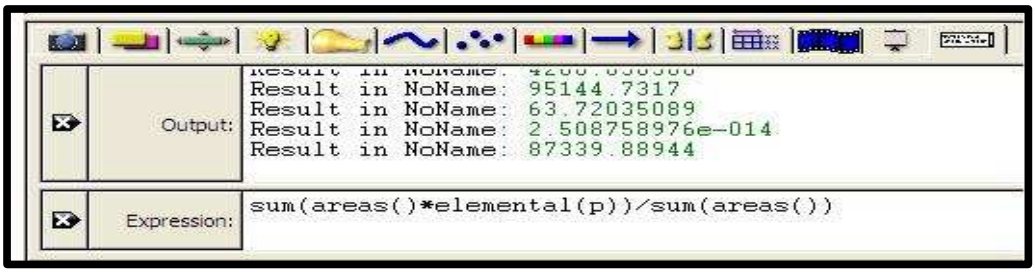

Figure 18. Output window

8.2 Simulation Results

Table 8. % Pressure loss in the duct may hence be calculated using the following formulae Eqn 30

Parameter	Inlet	Outlet
Density (Kg/m3)	0.957	0.9916
Mach No.	0.435	0.316
Pressure (Pa)	70119.68	68506.263
Temperature (K)	268.0	270.28
Velocity U (m/s)	141	26.39

Boundary conditions and pressure loss at mach 0.1 ie 1.05%.

8.3 Pressure Loss at Different Flight Conditions at 10000ft

Table 9. Total Pressure Loss at Several Flight Conditions at 10000ft

Cruise Speed (Mach No.)	0.1	0.2	0.3	0.4
Mass Flow Rate (lb/s)	3.555	3.555	3.555	3.555
CFD Input pressure (Pa)	70119.68	71650.32	74173.8	77807.34
Output pressure(Pa)	68506.263	70417.93	73320.80	76990.36
pressure loss (%)	1.05	1.15	1.72	2.3

$$\frac{P_{01} - P_a}{P_{01}} * 100 \qquad \text{Eqn. 30}$$

Pressure loss is $$\frac{70119.68 - 68506.263}{70119.68} * 100 = 2.300\% \qquad \text{Eqn. 31}$$

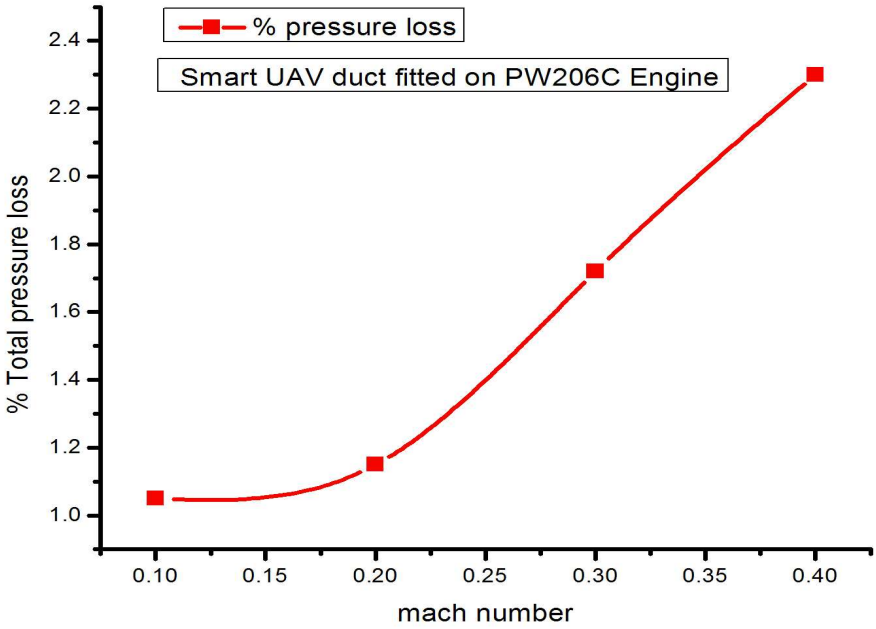

Figure 19. Pressure loss at 10000ft at different Mach number

According to the results pressure loss is experienced with increasing mach number.

8.4 Pressure Distribution

As previously mentioned in the abstract CFD has advantages of being able to analyze and see factors like flow field, pressure and temperature distribution within the model.

The following diagram represents the graphical output of the simulation that was performed at mach 0.4 10000ft free stream and 4° angle of attack.

Pressure build up represented in red and pink colors is realized, along the stagnation points around the elbow interface plane and the plenum chamber.

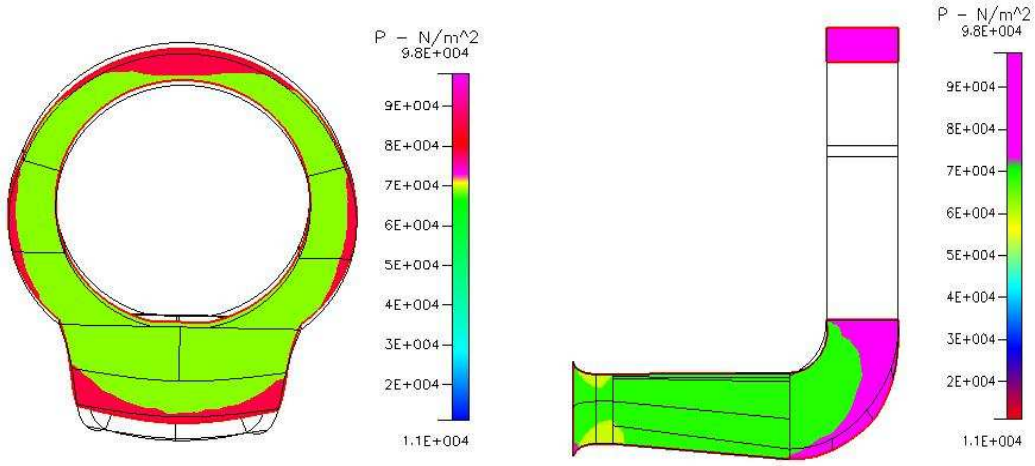

Figure 20. Pressure distribution inside inlet duct

This shows pressure distribution within the duct areas with red and pink are pressure stagnation points.

8.5 Temperature Fluctuation

Ambient temperature is an input boundary condition parameter that affects performance by controlling TIT turbine inlet temperature.

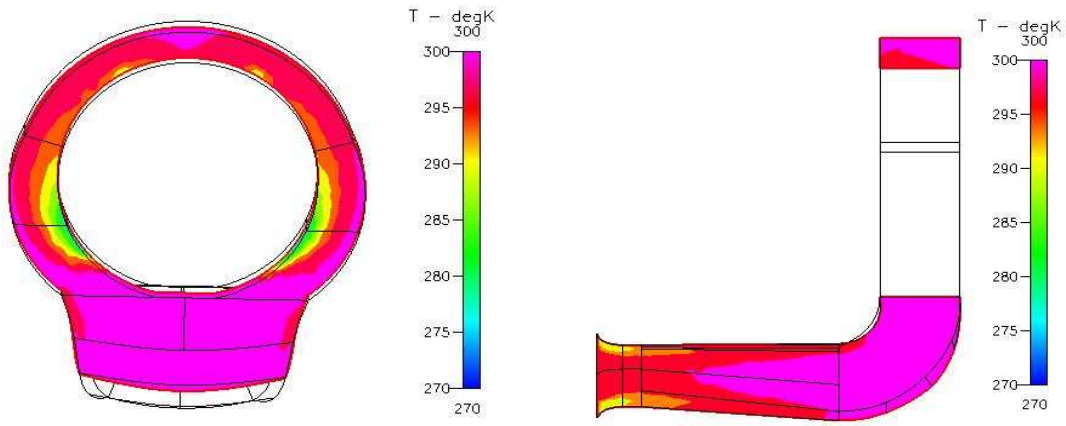

Figure 21. Temperature distribution in inlet duct

8.6 Flow Field

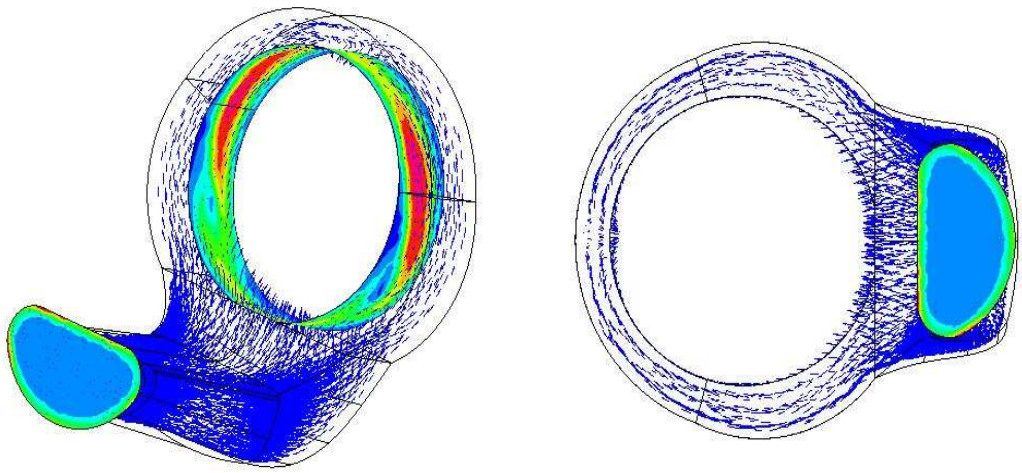

Figure 22. Flow distribution along duct and plenum chamber

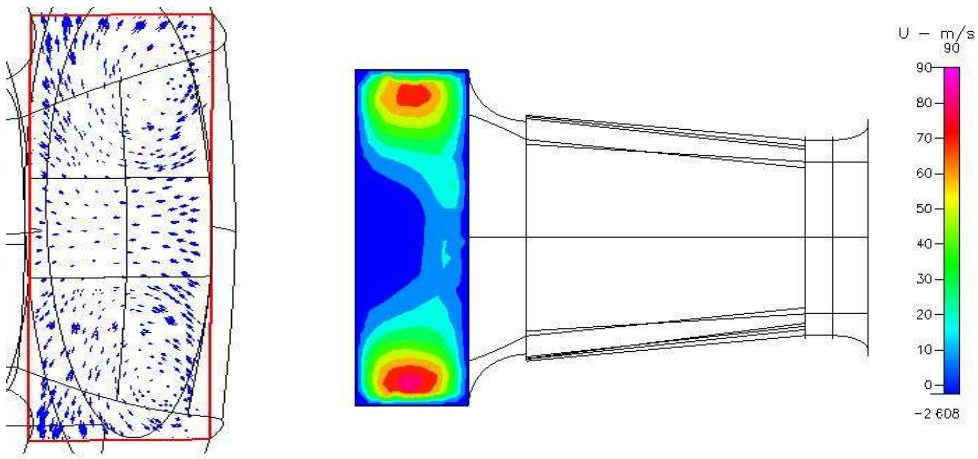

Figure 23. Graphical view of flow distortion

This figure shows the pressure distortion at the interface plane of the duct where flow enters the plenum chamber to the compressor face Figure 23.

9. EXHAUST DUCT

The exhaust duct is the end component that introduces the exhaust gasses into the atmosphere just like the intake duct its design is of vital importance to realize optimum performance.

The purpose of exhausted nozzle is to increase the velocity of the exhausted gasses before discharge and also to collect and straighten the gas flow.

The pressure ration across the nozzle controls the expansion process and the maximum thrust for a given engine is obtained when the exit pressure p_e is equal the ambient pressure p_0 .

The function of the nozzle may be summarized by the following

- Accelerate the flow to a high velocity with minimum total pressure loss
- Match exit and atmospheric pressure
- Allow cooling of walls if necessary
- Mix core and by-pass streams
- Do all the above with minimum cost ,weight , and boat-tail drag , while meeting life and reliability goals

Convergent nozzles are the most used for subsonic aircraft where the nozzle pressure ration p_{te}/p_0 is mostly less than 4.

9.1 Engine Back Pressure Control

The throat of a nozzle is one of the main means available to control the thrust and fuel consumption characteristics of the existing engines.

In preliminary engine cycle analysis, the selection of the specific values for the

engine design parameters and the design mass flow rate fixes the throat area of the nozzle.

At times it is necessary to change the off design operation of the engine in only a few operating regions and variation of the throat area of the exhaust nozzle may provide the necessary changes at reduced engine corrected mass flow rates (normally corresponding to reduced throttle setting) steady state operation close to the stall and surge line is not desirable since transient operation may cause the compressor to stall or surge.

The operating line can be moved away from the stall or surge by increasing the nozzle throat area. hence reducing the engine back pressure and increase the corrected mass flow rate through the compressor.

The study of the exhaust system looks at the analysis of high temperature internal flow of the exhaust system of the UAV. Its complicated flow pattern of the gas temperature in the internal system of the duct is analyzed using CFD tool where both the output results and appropriate formulas are used to determine the loss incurred in this design of duct.

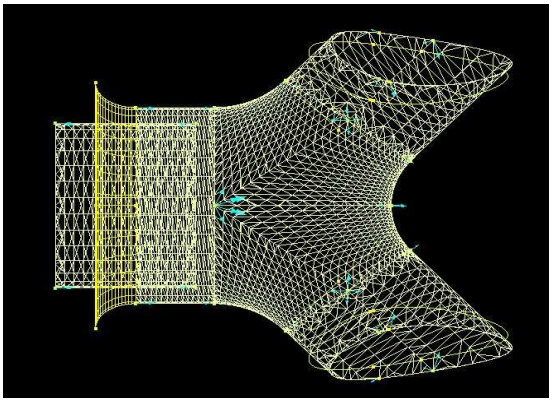

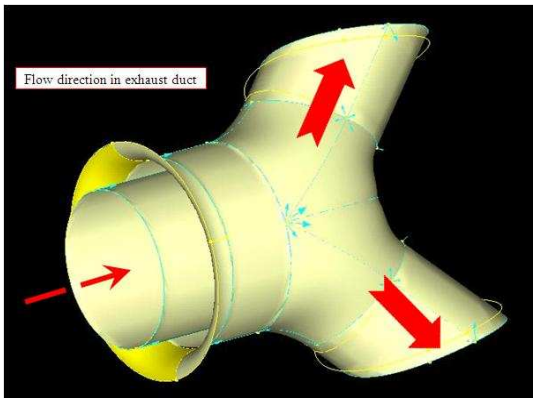

Figure 24. Exhaust duct mesh & flow direction

9.2 Modeling and Grid Generation

The process of grid generation is more like that for the intake duct structured grid was used with about 20000 elements. Two sets of inlet boundary conditions were used the core hot duct and cooling air duct.

The core inlet receives hot gasses at 868.86K (TET) projected at 160m/s and total inlet mass flow rate (3.555Lb/s) that remains constant following conservation of mass law and through components matching.

The boundary conditions used for exhaust duct include off-design point simulation result values of T_2 and P_2, mass flow from engine turbine outlet.

Delta T from ISA	R	0
Relative Humidity [%]		0
Mach Number		0.4
Shaft Power Delivered	hp	559.736
Power Sp. Fuel Cons.	lb/(hp*h)	0.497609
Specific Power	hp/(lb/s)	157.461
Handling Bleed WB_hdl/W2		0
Total Overboard Bleed	lb/s	0
Total Rel Overb Bleed W_bld/W2		0
Fuel Flow	lb/s	0.0773692
HP Turbine Pressure Ratio		3.04641
PT Pressure Ratio		3.28994
Ambient Pressure Pamb	psia	10.1065
Inlet Temperature T2	R	498.491
Inlet Pressure P2	psia	11.2847
Intake static Pressure Ps2	psia	0
Compressor Exit Temp T3	R	1048.26
Compressor Exit Press P3	psia	106.859
Compr Exit static Press Ps3	psia	102.239
Burner Exit Pressure P4	psia	103.607
Burner Exit Temperature T4	R	2397.94
Stator Outlet Temp T41	R	2397.94
HP Turbine Exit Temp T44	R	1937.76
HP Turbine Exit Press P44	psia	34.0096
PT Inlet Pressure P45	psia	34.0096
PT Turbine Exit Temp T5	R	1538.11
PT Turbine Exit Press P5	psia	[illegible]

Point 1 selected

Figure 25. Off design mission analysis output

This figure above represents mission analysis results done at 10000ft and mach number 0.4. It is at this state that maximum continuous turbine exit temperature (TET) is realized and the cooling stream is at its maximum flow.

Table 10. Exhaust duct simulation results

Hot gas inlet	Inlet	Outlet
Temperature (K)	868.86	626.8
Mass flow rate (Lb/s)	3.555	Both exit 3.981
Pressure (Pa)	71271.1	70202.33

The difference in mass flow rate at the outlet is due to cooling air from outside of about 0.4466kg/s being the reason for temperature decrease to 626.8(K).

% pressure loss hence may be calculated as $\frac{P_{01} - P_a}{P_{01}} * 100$ Eqn. 32

Substituting value on Table 9 Loss= 1.499%

Pressure distribution in the exhaust duct can be seen on Figure 42 Appendix B.

10. ENGINE LOSS

10.1 Description

Performance targets are usually stipulated as un-installed, with the engine performance quoted from the engine intake flange to the engine exhaust or propelling nozzle flange.

If performance targets are installed then installation effects such as the ones below are considered.

- Intake pressure loss
- Jet pipe pressure loss
- Accessory power requirements
- Bleed off take
- Shaft power out put
- Specific fuel consumption (SFC)

10.2 Installed and Un-installed Performance

The study begins by first performing out the design and off-design performance analysis of the PW206C engine at which point work and mass flow within the engine components are iterated and converged.

Since the performance is done using a commercial program (GASTURB 9) the accuracy and closeness of the output data must be verified. This is done by referring and comparing data with those from the manufactures deck EEPP program provided by the manufacturer to engine owners.

From the simulation the engine converged at a design point performed at 10000ft, Mach 0.4.

10.3 Un-installed Condition

Plots of the engine thrust, thrust specific fuel consumption and engine mass-flow rate and flight Mach number and altitude are usual ways that the Un-installed engine performance in presented.

1. Pressure loss at inlet and exhaust duct were ignored
2. Bleed air and accessory gearbox power extractions were not considered

Three variations were considered during this analysis.

Table 11. Variations considered at un-installed condition

Gas generator rpm (%)	60	70	80	90	100
Altitude (ft)	5000	10000	15000	-	-
Mach number	0	0.1	0.2	0.3	0.4

Simulated values of mass flow rate, fuel flow rate, shaft horse power was plotted against variations on Table 11 above compared to respective values got from the EEPP.

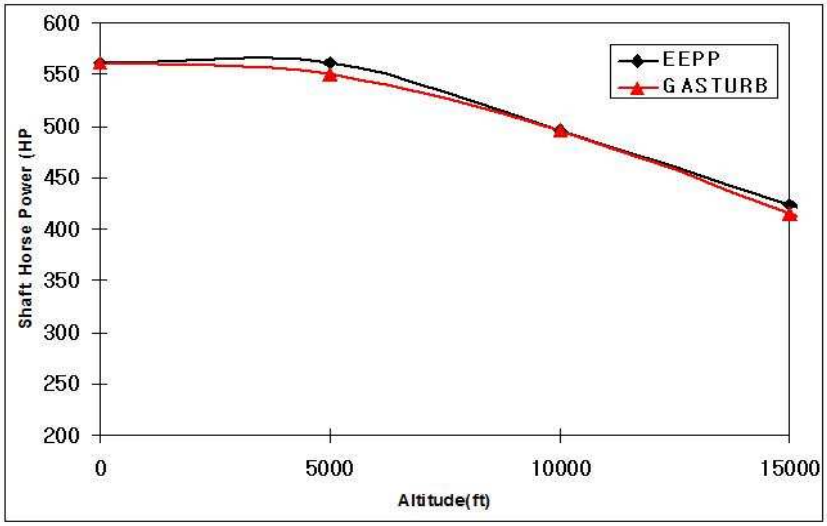

Figure 26. Un-installed loss with altitude variation

The shaft power reduces gradually as the altitude increases towards 15000ft the trend is observed in both value got from EEPP and Gasturb 9 this data were obtained as a result of changing the altitude at design point in between 0~15000ft and getting the corresponding shaft horse power at mach 0.4, 100%RPM of generator speed.

The Figure 27 below shows variation of mach number following the similar procedure where mach number was varied at an interval of 0.1 between 0~0.4 at an altitude of 10000ft, carried out at 1000ft gas generator speed of 60% was maintained.

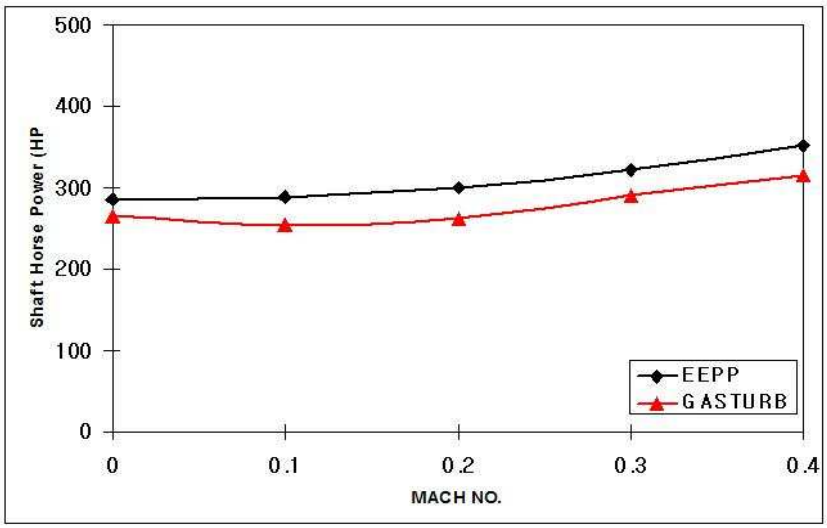

Figure 27. Un-installed loss with mach number variation

Corresponding values of shaft power was noted and plotted values from the EEPP program was used as a point of comparison. As the mach number increase then shaft horse power increases. Shaft horse power increases with increasing gas generator spool speed. in this case the analysis was performed at sea level static condition, Mach number 0.4. see Figure 28.

More graphs of fuel flow rate, mass flow rate may be found in the Appendix.

A.

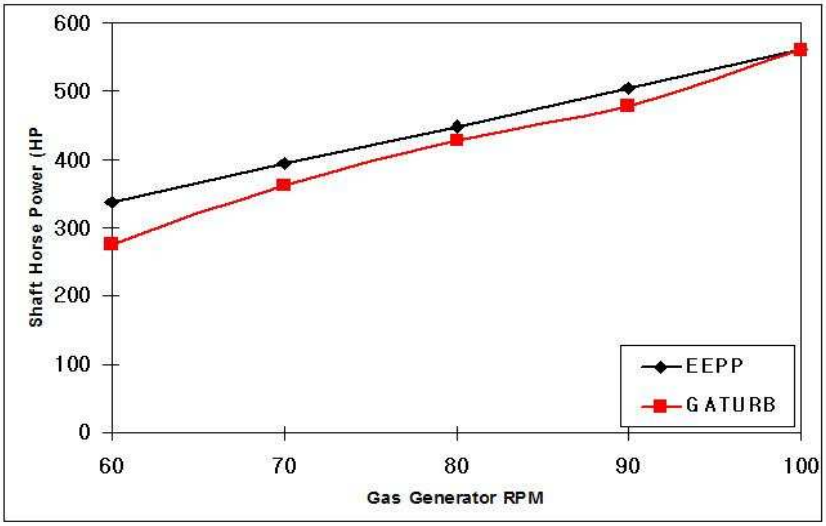

Figure 28. Un-installed loss with gas generator variation

10.4 Installed Condition

Installed loss as described above considers several loss factors inlet and exhaust loss analysed in this thesis using CFD tool together with other loss parameters are collectively used to do the analysis.

The losses considered are seen on Table 12 below.

Table 12. Losses considered at installed condition

Loss parameter	ECS OFF	ECS MAX	Un-Installed Condition
Inlet efficiency	1	0.9922	1
Inlet temperature rise	5R	5R	0
Bleed air loss	0	5%	0
Power extraction	5HP	7HP	0
Intake loss	2.3%	2.3%	0
Exhaust loss	1.499%	1.499%	0

This assumptions were made at environmental condition off and environmental condition at maximum. Since the aircraft cabin needs to nature environmental condition that are friendly to human survival air conditioning is necessary bleed air from the engine hence may be used.

The engine drives several peripheral devices necessary for good engine performance or starting this devices extracts some power to run and overcome mechanical inefficiencies like friction and so on.

Corresponding values of shaft horse power mass flow rate and fuel flow rate were plotted against mach number, gas generator RPM and altitude at both ECS at MAX and OFF and at un-installed conditions.

Table 13. Variations considered at installed condition

Gas generator rpm (%)	60	70	80	90	100
Altitude (ft)	5000	10000	15000	-	-
Mach number	0	0.1	0.2	0.3	0.4

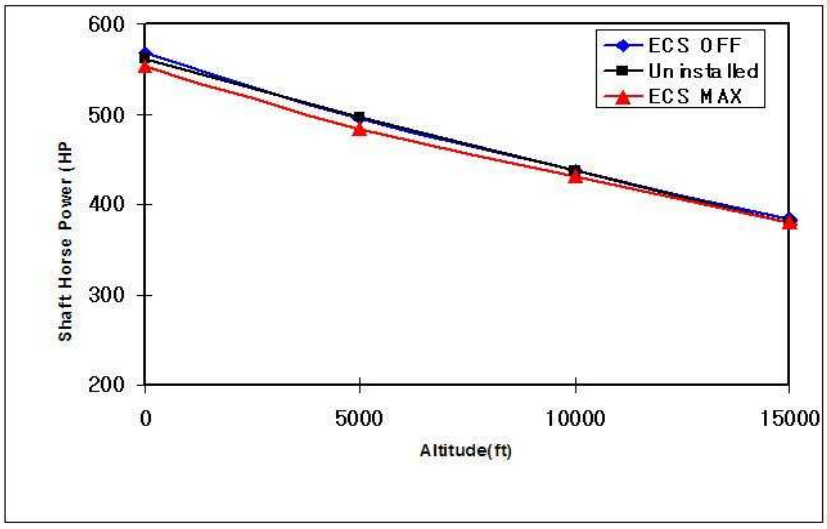

Figure 29. Variation of altitude at installed condition

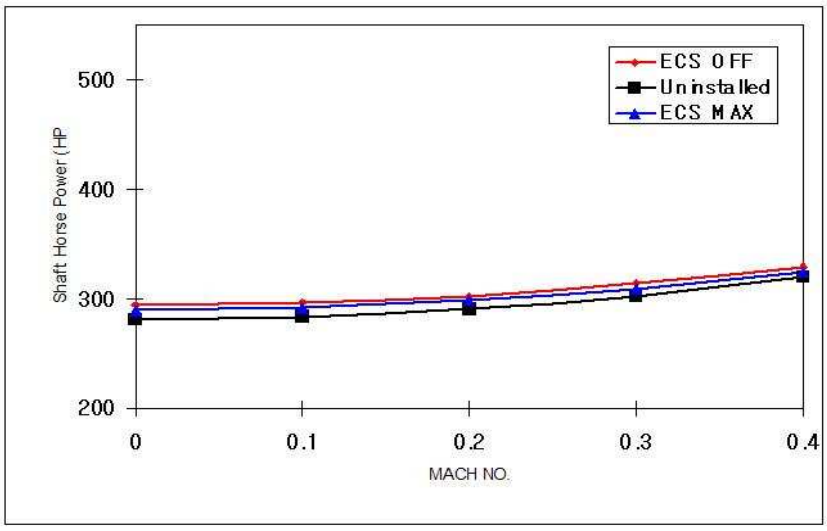

Figure 30. Variation of mach number at installed condition

Shaft horse power reduces with increasing altitude their is a slight loss of power at ECS max due to losses incurred as a result of power extraction and changes in air density, hence mass flow rate both Mach number and Gas generator RPM were maintained at 0.4 and 100% respectively.

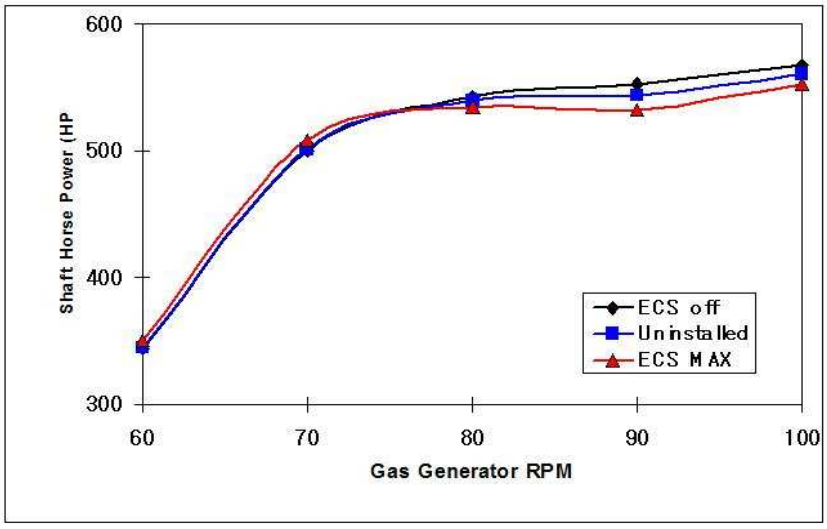

Figure 31. Gas generator speed variation at installed condition

Variation of mach number figure 30 above was done at a design point of 10000ft. Since increase in mach number increases the mass flow rate we realize power increase towards mach 0.4 it applies to all the cases where ECS is off and at MAX although slight loss at ECS max due to mechanical losses and so on at gas generator RPM of 60%.

Figure 31 was also performed at Sea level static condition and Mach number 0.4 where change in RPM yielded corresponding value of shaft horse power that were plotted against RPM between 60~100% . Shaft horse power increase constantly until 100% RPM that gives shaft horse power of about 550 rated power.

As expected when ECS is at max their is slight power loss due to the several reasons noted above.

More performance graph are found in the Appendix B.

11. SOURCES OF ERROR

CFD accuracy the associated errors that arise from use of computational simulation tool are simple but not necessarily qualifiable. The programme requires the user to insert the known constants and engine specifications, but at no point is an actual physical geometry specified. Therefore, even with changes of engine specifications relative to the engine of interest, other effects due to exterior and intake geometry are not considered.

In the example used in this paper, the PW206C engine uses an intake duct that is not symmetrical in the x-y plane, ie, the upper lip and lower lip of the intake are different size and shape.

CFD program has no function to input this into the code, a generic engine with intake lips of equal size and shape is assumed and this will lead to a qualitative error in the flow calculation of the ingested air.

its however very difficult to eliminate this error as the actual flow differences needs that the geometry be defined prior to simulation. it is therefore assumed that an error exists , but is not quantified in this paper.

11.1 CFD Mesh and Solver

The use an unstructured grid, for production of the mesh, automatically leads to reduction in accuracy of the CFD solver. this is due to an unstructured grid mesh not capturing the geometry exactly and unfortunately ignoring some of the curved surfaces and highly complex shapes. It is possible to increase the effectiveness of unstructured grids, by increasing the density by a large factor, but this also increase the run-time for each simulation of each condition. as many simulation are needed for convergence and performance estimations it is good practice to make a compromise between accuracy and length of run-time. Therefore by choosing a

fairly high density, unstructured mesh compromise may be made. Alternatively use of structured mesh that has the same effect may be done.

The turbulence model of choice in this example is the $k-\epsilon$ model with a turbulence intensity of 1% and turbulence viscosity ratio of 1. a higher order model with higher intensity ratio may have been used but because of a choice dominated by time criteria the use of the current model is again the correct compromise, between run-time, convergence and accuracy.

12. CONCLUSION

This paper describes a technology strategy for advanced engine simulation utilizing the use of computational fluid dynamics. It is through this techniques that component performance data can be efficiently and reliably simulated in a way that its flow field is visible in 3-D, pressure, temperature and other parameters associated with fluid dynamics may be made cheaply, faster and at a fairly accurate manner.

The work in this paper describes the accuracy of the CFD generated performance results strongly depends on the quality of the CFD model geometry, grid quality and definition of boundary conditions in the CFD solver.

The analysis described inn this paper was carried out at straight and level with a fixed TET setting was maintained whilst the Mach number varied from 0～0.4 and altitude from 0～10000ft for CFD simulation and slightly higher in installation loss analysis.

A detailed comparison between the engine performance predicted by fixed pressure recovery value and the performance simulated using CFD generated duct losses were analyzed and compared for varying altitudes ,Mach number and Gas generator spool speed.

The results presented in this paper are fairly accurate regardless of the various sources of error mentioned. It may be concluded therefore that the use of CFD to analyse engine components is justified and more detailed understanding of the program may further improve its accuracy.

REFERENCE

[1] Victoria Nichols "The effect of distortion on intake of a civil aero engine using a fully integrated to zooming" (Thesis Cranfield 2005)

[2] ChangDuk Kong "Component map generation of gas turbine engine using engine performance deck" (ASME 2006)

[3] J. Kurzke "Effect of inlet flow distortion on performance of gas turbine" (ASME 2006)

[4] George "analysis of installed and un-installed performance of turbo shaft engine" (24Th KSPE)

[5] Asim Maqsood "Experimental and CFD study of exhaust ejectors with bent mixing tubes" (ASME 2005)

[6] Intake Aerodynamics, second edition Blackwell science, J Seddon & E,L Goldsmith & J Seddon 1993.

[7] NASA Education www:// nasa. gov

[8] Practical intake Aerodynamic Design ,Black Scientific Publications Oxford E. L Goldsmith & J Seddon 1999.

[9] Design and Off Design simulation handbook ,Gasturb 9 ,J Kurzke.

APPENDIX A

Un-installed Condition Performance Curves

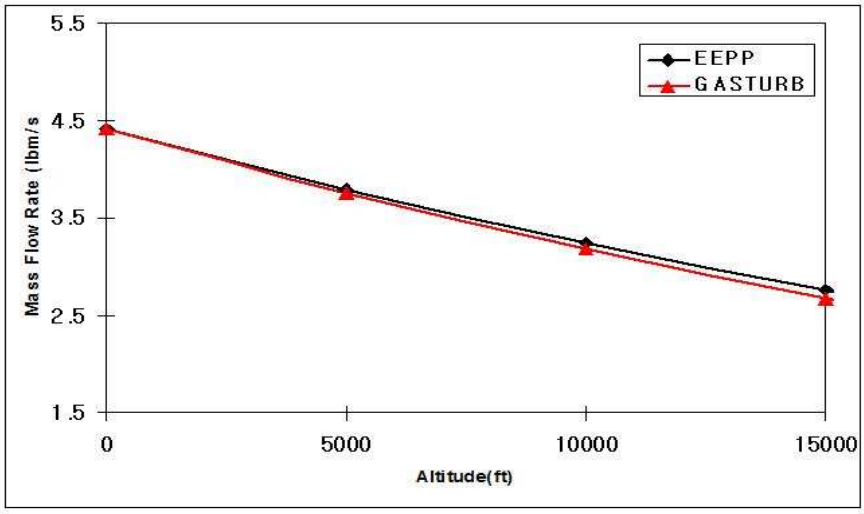

Figure 32. Variation of altitude with 100% gas generator speed Mach 0.4

Mass flow reduce with increasing altitude due to change in density.

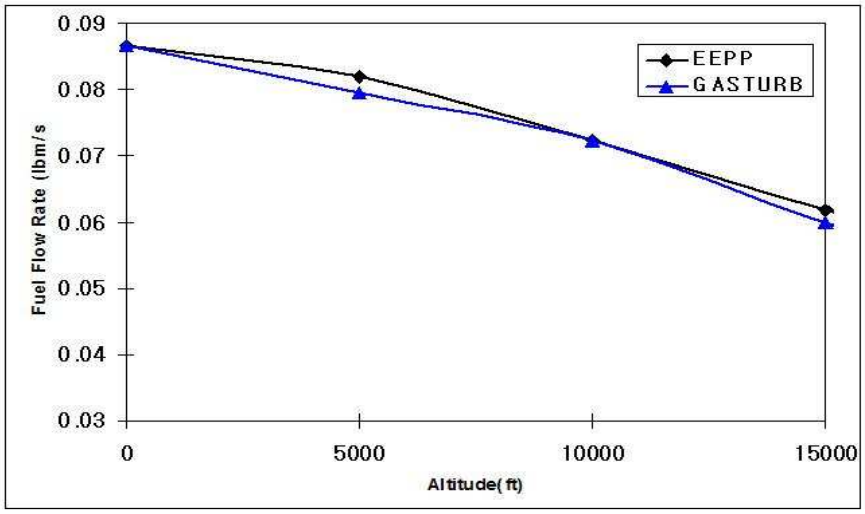

Figure 33. Variation of altitude with 100% gas generator speed Mach 0.4

Fuel flow rate reduces with increasing altitude and follows the contours of the results given by EEPP.

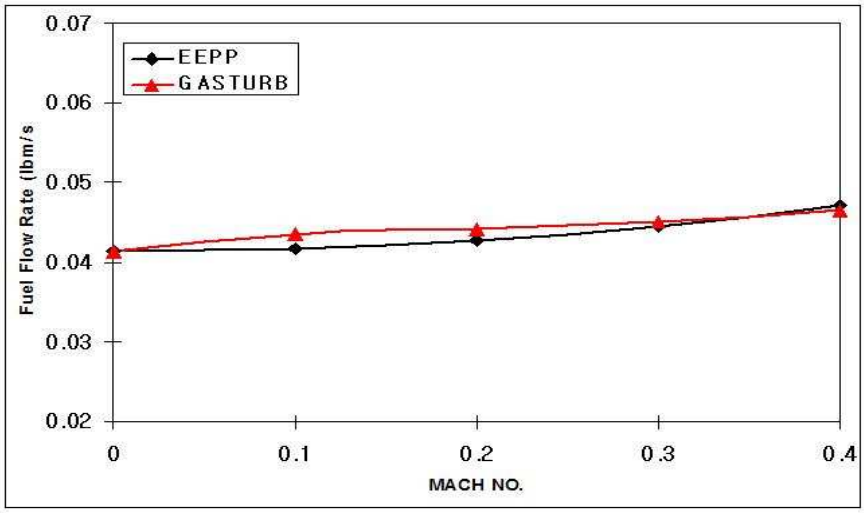

Figure 34. Variation of Mach number with 60% gas generator rpm at 10000ft

Both fuel flow are the same at the design point where mach number is 0 the difference at mach number 0.2 and 0.3 may be attributed to difference in efficiencies.

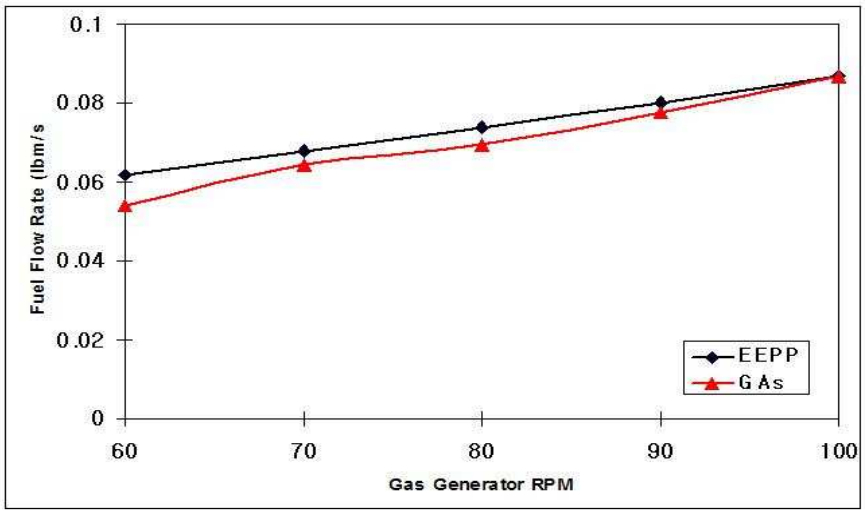

Figure 35. Variation of gas generator rpm at Mach 0.4, altitude 10000ft

Fuel flow rate increase with increasing Gas generator speed.

APPENDIX B

Installed Condition Performance Curves

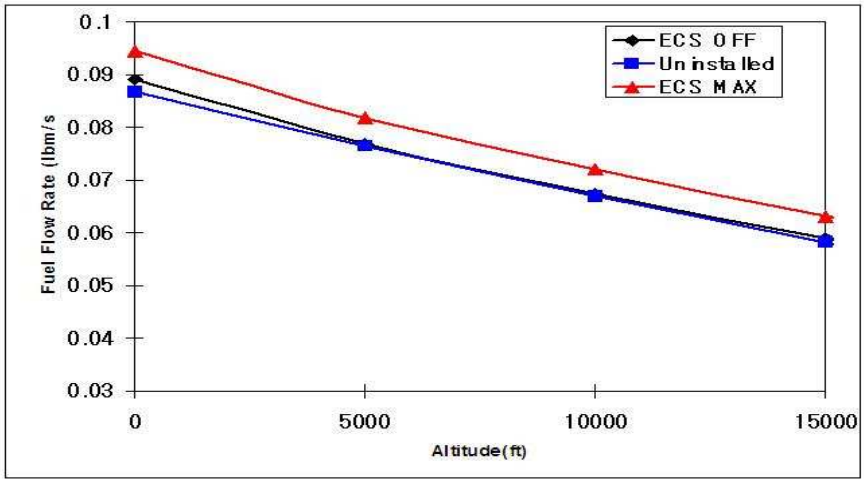

Figure 36. Installed loss performed at Mach number 0.1, gas generator rpm 100%

Fuel flow increases at ECS MAX due to bleed air extraction.

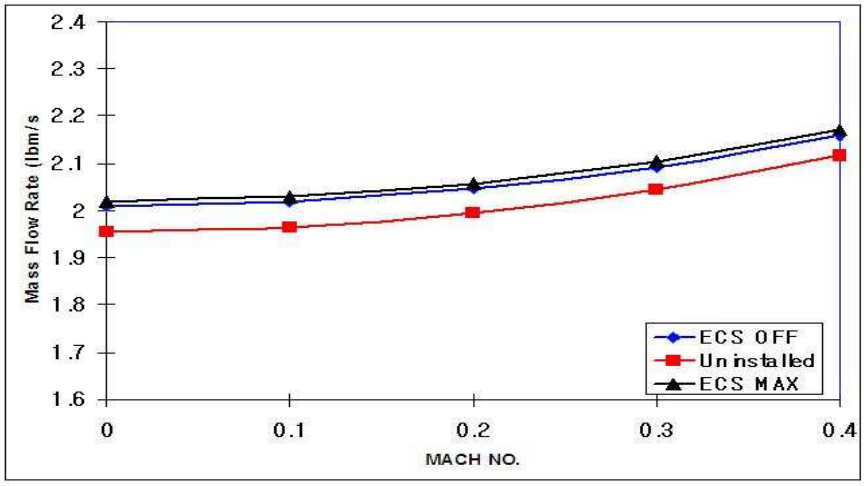

Figure 37. Installed loss performed at gas generator rpm 100% at altitude 10000ft

Mass flow increase as it is a function of speed density and area.

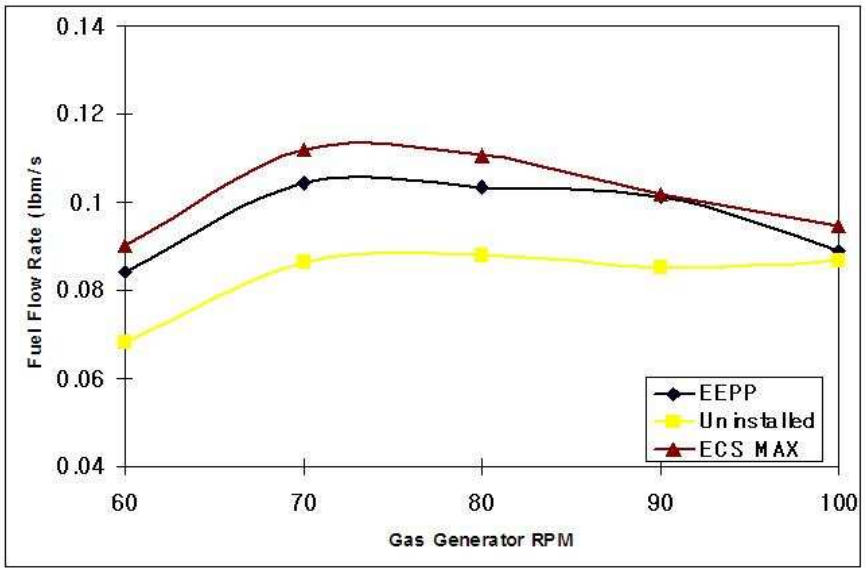

Figure 38. Installed loss performed at sea level static, gas generator rpm 100%

Gas generator speed increases fuel flow slightly where it then settle to lower point at 100% may be linked to increase in mechanical loads.

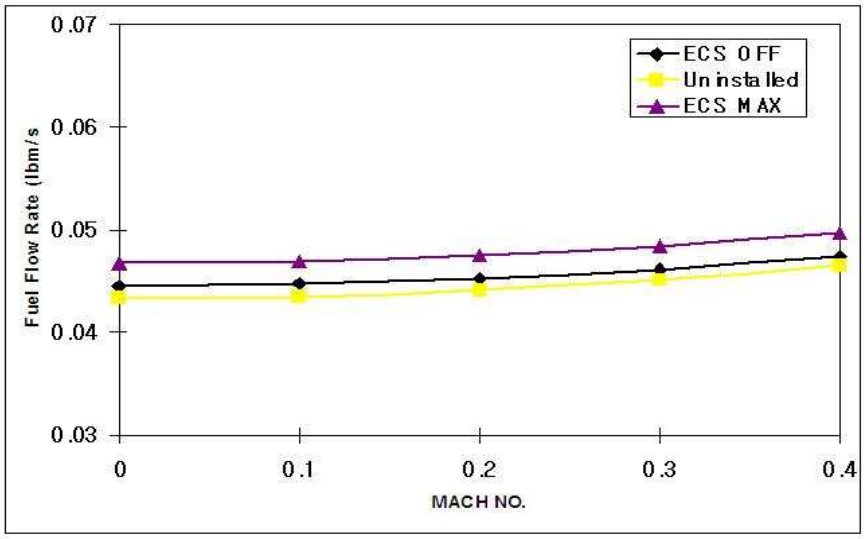

Figure 39. Installed loss performed at Mach number 0.1 at altitude 10000ft

Although not much increasing mach number increases fuel flow to compensate for the addition work done by the compressor in handling additional air mass flow.

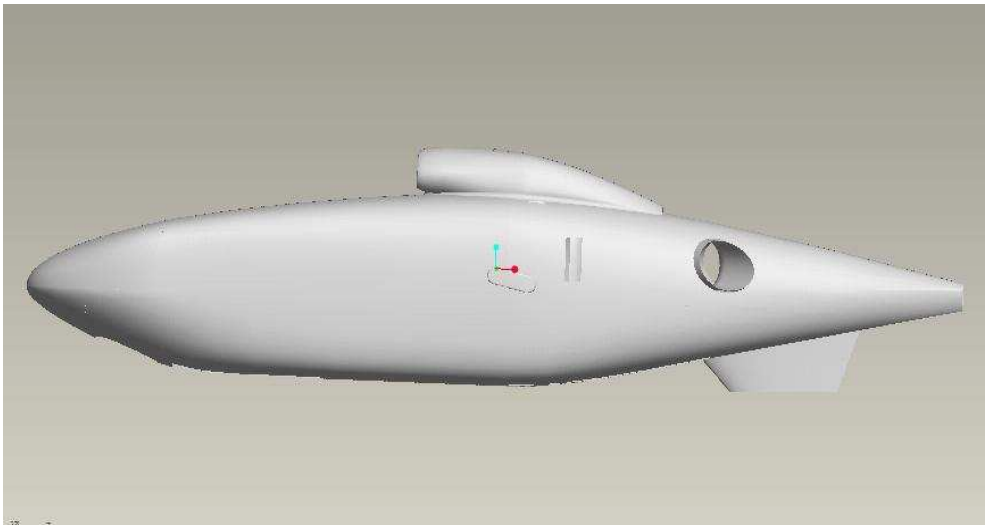

Figure 40. Inlet and exhaust position on the airframe involved

Represented here shows the intake on the upper surface and side exhaust duct.

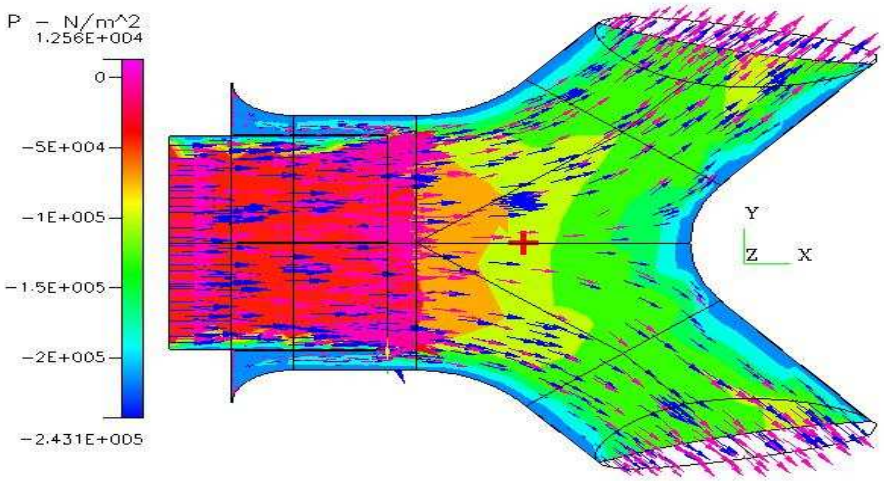

Figure 41. Pressure distribution in the exhaust duct